

# Addressing Source Scale Bias via Image Warping for Domain Adaptation

Shen Zheng\* Anurag Ghosh\* Srinivasa G. Narasimhan  
 Robotics Institute, Carnegie Mellon University  
 {shenzhen, anuraggh, srinivas}@cs.cmu.edu  
<http://instancewarp.github.io>

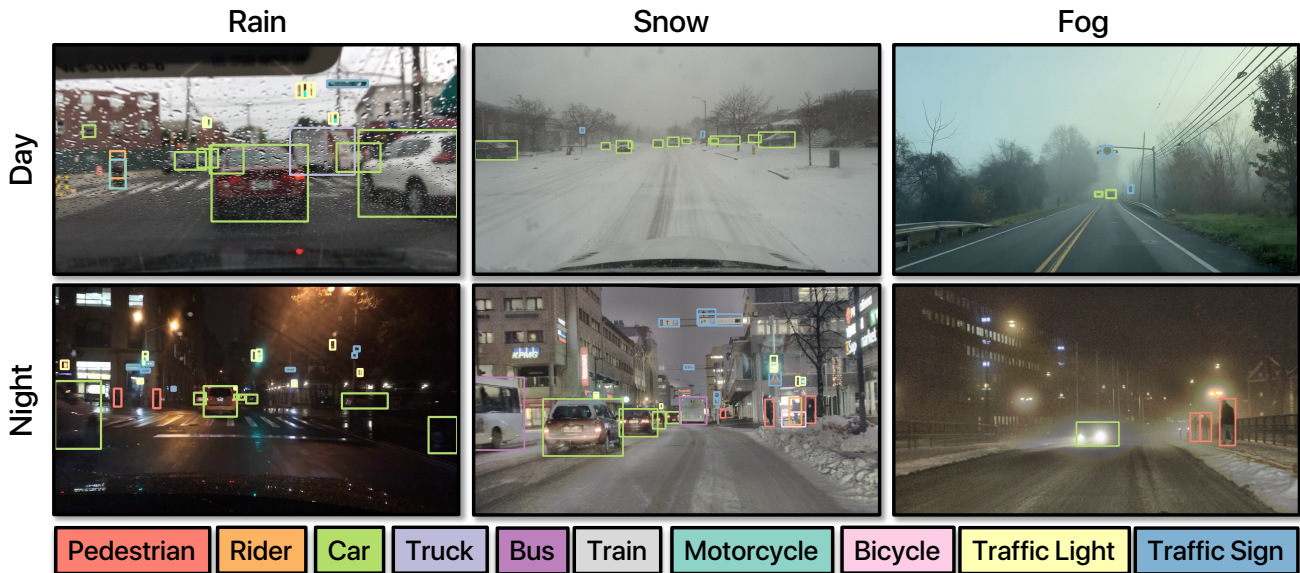


Figure 1. Our method improves domain adaptive object detection across a extensive range of lighting and weather scenarios in various target datasets (or subsets) using supervision from the BDD100K source subset containing day images in clear weather.

## Abstract

In visual recognition, scale bias is a key challenge due to the imbalance of object and image size distribution inherent in real scene datasets. Conventional solutions involve injecting scale invariance priors, oversampling the dataset at different scales during training, or adjusting scale at inference. While these strategies mitigate scale bias to some extent, their ability to adapt across diverse datasets is limited. Besides, they increase computational load during training and latency during inference. In this work, we use adaptive attentional processing – oversampling salient object regions by warping images in-place during training. Discovering that shifting the source scale distribution improves backbone features, we developed a instance-level warping guidance aimed at object region sampling to mitigate source scale bias in domain adaptation. Our approach im-

proves adaptation across geographies, lighting and weather conditions, is agnostic to the task, domain adaptation algorithm, saliency guidance, and underlying model architecture. Highlights include **+6.1** mAP50 for BDD100K Clear → DENSE Foggy, **+3.7** mAP50 for BDD100K Day → Night, **+3.0** mAP50 for BDD100K Clear → Rainy, and **+6.3** mIoU for Cityscapes → ACDC. Our approach adds minimal memory during training and has no additional latency at inference time. Please see Appendix for more results and analysis.

## 1. Introduction

Visual detection and segmentation of things (i.e. object instances) and stuff, across different scales is a fundamental challenge in computer vision [19, 35, 45, 49]. Natural scene

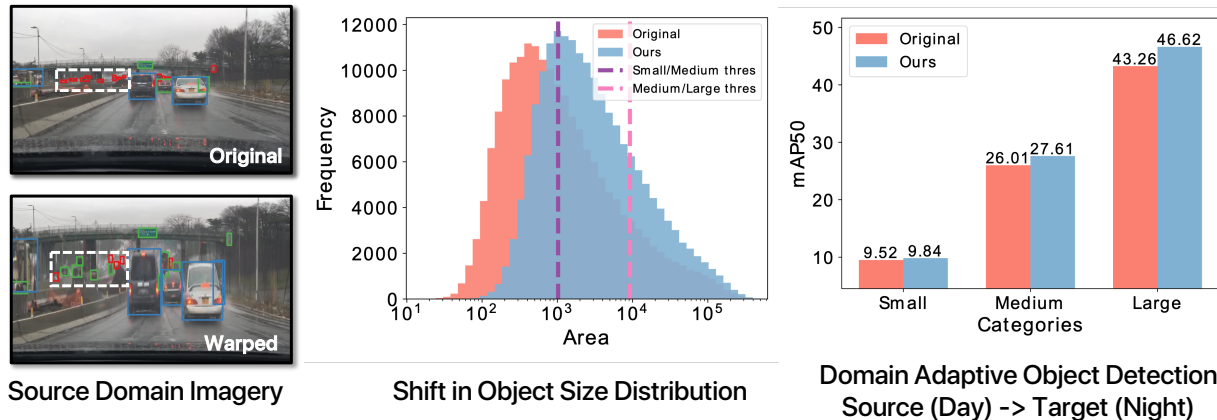


Figure 2. **Image Warping to Address Source Domain Scale Bias.** Bounding boxes mark **small**, **medium**, and **large** objects in the image. Driving scenes contain many objects that appear small in the image, some objects that have medium image sizes, and few objects that appear large. Our approach shifts this unbalanced scale distribution in datasets by oversampling medium and large-sized objects to address the scale bias.

datasets used for training different tasks often exhibit bias of imaged objects towards certain scales (or sizes). For instance, in autonomous driving situations, camera perspective and field of view warrant that many more distant objects that appear small in the image are captured compared to nearby objects that appear large, even if the real object 3D scale distribution is near-uniform. This results in an inherent imbalance or bias in the distribution of sizes of object projections in the image, leading to sub-optimal recognition models.

Common approaches to address scale bias are: (a) selecting an image subset to create a uniform scale distribution but this is suboptimal as only a fraction of the available data is used; (b) oversampling via data augmentation (e.g., multi-scale training [35] and multi-scale inference [10, 13, 34]), while helpful, also introduces significant computational and storage overhead; (c) introducing scale-invariance priors (e.g., feature pyramids [21–23]), but this only partially alleviates scale bias, as both things and stuff vary widely in scale and image locations.

We propose a new method to address scale bias, orthogonal to previous techniques, using adaptive attentional processing. We warp images *in-place* while training models to shift the unbalanced scale distribution of objects (see Figure 2). While non-uniform warping techniques, i.e. allocating more pixels using a predefined guidance, have been applied to improve image classification [25], detection [7, 9, 36, 37] and segmentation [37] in supervised settings, they do not principally examine and address the scale bias for domain adaptation.

We propose Instance-level Saliency Guidance which analytically shifts the object scale distribution to remove bias or match target distribution by leveraging ground truth labels for maximum performance gain. Because the warp-

ing is in-place, we directly re-sample objects (e.g. expand smaller ones) and squeeze the large empty regions in the scene (e.g. road), allowing for a better use of the image pixel budget for balanced distribution training. We show that this warping improves backbone features of our model crucial for domain adaptation. To make sure our outputs are in the original unwrapped configuration, we unwarp the features, as in LZU [37], and train without warping the object labels. During inference, no warping is performed and the method requires no additional computational latency. Our contributions are highlighted as follows:

- We are the first work to show that scale bias in real-to-real domain adaptation can be effectively addressed through image warping, and that shifting source scale distribution significantly improves backbone features.
- Our approach is agnostic to task (detection or segmentation), adaptation strategy, model architecture and warping guidance used for sampling.
- Our approach improves domain adaptation across various lighting (+3.7 mAP50 for BDD100K Day → Night detection), weather conditions (+6.1 mAP50 for BDD100K Clear → DENSE Foggy detection), and geographies (+6.3 mIoU for Cityscapes → ACDC semantic segmentation). See Figure 1.
- Our approach is efficient: we introduce train-time image warping and feature unwarping for domain adaptation without need for test-time warping. This results in minimal training overhead and *no additional inference latency*.

## 2. Related Work

**Alleviating Scale Bias.** Recognition across different scales is a historically important problem. Priors that encour-

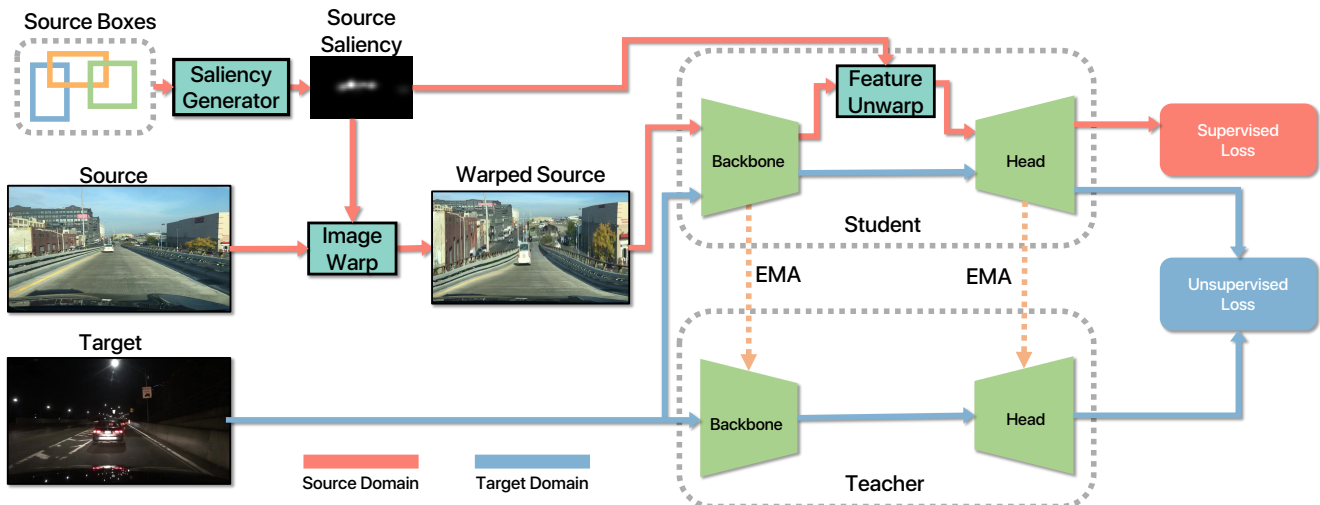


Figure 3. **Warping for Domain Adaptation.** Consider the Unsupervised Domain Adaptation setting (like [12, 17]), which adapt from source domain to target domain in 2 stages – a supervised pre-training on the source domain and an unsupervised adaptation stage from source to target. Components of our method are marked in cyan. For a source domain image, we generate a saliency guidance based on the dataset’s scale distribution and source bounding boxes (Section 3.2) to decrease scale bias and unwarp the features before computing the supervised loss in the *unwarped* label space. Guidance could instead be computed via Static Prior [36, 37] or Geometric Prior [9], but our Instance-Level Guidance performs better and with no test-time latency (Sections 5.1 and 5.2). Unsupervised losses computed on the target image of the Domain Adaptation Algorithm (say from [6, 12–14, 17, 18, 48]) remains the same.

age scale invariance like feature (or anchor) pyramids are widely used in pre-deep-learning approaches [5, 23] and recently [21, 22, 27]. While helpful, these priors do not solve scale bias completely, as an object can be bigger or smaller than pre-defined scales. Common augmentation techniques such as multi-scale training [13, 17, 27, 35] can considerably increase training time. Similarly, test time scaling [10, 34] and multi-scale or multi-crop predictions [13, 26] improve accuracy at the cost of latency and memory [15]. Another line of works select “optimal” scale at inference [3, 8], but don’t improve the learned model itself. Compared to earlier work, our method explicitly addresses scale bias requiring (a) little additional memory during training since we warp images in-place; and (b) no additional inference latency as we do not warp during testing. Crucially, our approach is orthogonal to other scale bias reduction techniques, and can be used in a plug-and-play manner.

**Guided Image Warping.** Non-uniform Spatial Transformations [42] have been used to correct image distortions arising from camera acquisition. Recently, spatial transformation methods [16, 25] for learned models have advocated introducing image distortions instead. Learning to Zoom [25] showed over-sampling task-specific salient regions is useful as visual recognition requires combining information from different spatial resolutions. Building on this paradigm, warping for other tasks like detection [36,

37] and segmentation [37] were explored. Fovea [36], and Two Plane Prior [9] designed “salient” priors to guide warping, introducing static & temporal, and geometric saliency guidance respectively.

Our approach stands out in the following ways: (a) Unlike previous image warping efforts focusing on supervised settings, our innovative training strategy and saliency guidance tailor image warping for unsupervised domain adaptation to directly address scale bias. (b) Unlike former image warping methods that indiscriminately process objects and background elements, we introduces an analytical instance-level saliency guidance that targets regions containing objects.

**Image Transformations for Domain Adaptation.** Image Transformations like flipping, cropping, blurring, color jittering, grayscaling, contrast adjustment are widely used as perturbations for domain adaptation [6, 11–14, 17, 18, 24, 31, 38, 39, 41, 43, 45, 46, 48] to increase source domain diversity and decrease domain gap to the target domain. For example, 2PCNet [17] introduces a domain-specific Night Augmentation (NightAug) pipeline that attempts to make day images appear closer to night images. To the best of our knowledge, in-place image warping as a domain adaptive perturbation has not been explored in prior works. Our approach is agnostic to the specific domain adaptation training algorithm, and can be easily incorporated with any other augmentation strategy.



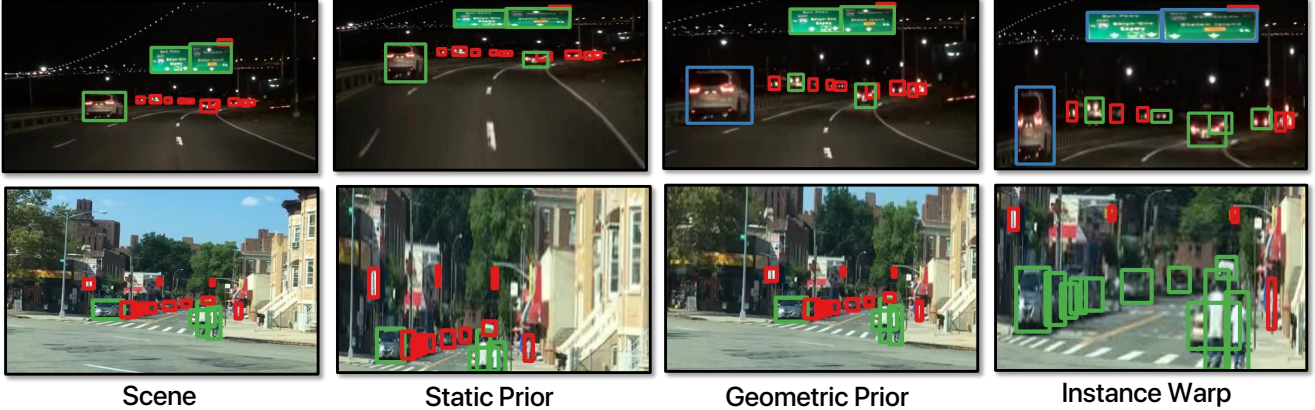


Figure 4. **Image Warping with Different Priors.** In-place warping follows a zero-sum pixel constraint: *enlarging one region necessitates shrinking another*. Bounding boxes mark **small**, **medium**, and **large** objects in the image. Our method specifically targets object instances. In comparison, the Static Prior fails when instance distribution deviates from the dataset average, whereas the Geometric Prior fails for small objects unaligned with the dominant vanishing point.

### 3. Method

We first describe how we warp images assuming a spatial guidance function while remaining task agnostic. Then, we design our warping guidance that can explicitly address scale bias (as shown in Figure 1). Finally, we detail how to train models with warped images that adapt better to new domains. The entire strategy is illustrated in Figure 3.

#### 3.1. Image Warping and Feature Unwarping

We employ the saliency guided sampling mechanism from [25]. However, other methods may also be used (like thin plate spline transformations [7, 16]).

**Image Warping:** We consider an inverse transformation  $\mathcal{T}_S^{-1}$  parameterized by saliency  $S$  such that,

$$I'(\mathbf{u}) = W_{\mathcal{T}}(I) = I(\mathcal{T}_S^{-1}(\mathbf{u})) \quad (1)$$

a resampled  $I'$  for every location  $\mathbf{u}$  is obtained by using warp  $W_{\mathcal{T}}$  given input image  $I$  and saliency guidance  $S$ , which is a 2D map of the output image size. The rationale and choice of  $S$  is described in Section 3.2.

**Feature Unwarping:** If we operate in the space of warped images, our outputs would also be warped. However, we do not wish to warp our labels to match the input warped image, hence, we perform feature unwarping of spatial backbone features and train the model without warping our labels or unwarping our predictions, like [9, 36]. The benefit of this strategy is that it renders our warping mechanism task agnostic. We adopt the strategy from LZU [37], which approximates  $\mathcal{T}$  with  $\tilde{\mathcal{T}}$ , a piecewise tiling of invertible bilinear maps, and then perform feature unwarping via,

$$\mathcal{T}^{-1}(\mathbf{u}) \approx \tilde{\mathcal{T}}^{-1}(\mathbf{u}) = \begin{cases} \tilde{\mathcal{T}}_{ij}^{-1}(\mathbf{u}) & \text{if } \mathbf{u} \in \text{Range}(\tilde{\mathcal{T}}_{ij}) \\ 0 & \text{else} \end{cases} \quad (2)$$

We restrict the space of allowable warps for  $\mathcal{T}$  such that axis alignment is preserved. Entire rows or columns are “stretched” or “compressed” in this case, which has been observed to perform better [9, 36, 37]:

$$\mathcal{T}_{S,u}^{-1}(u) = \frac{\int_{u'} S_u(u') k(u', u) u'}{\int_{u'} S_u(u') k(u, u')} \quad (3)$$

$$\mathcal{T}_{S,v}^{-1}(v) = \frac{\int_{v'} S_v(v') k(v', v) v'}{\int_{v'} S_v(v') k(v, v')} \quad (4)$$

where  $k$  is a Gaussian kernel and  $\mathbf{u} = (u, v)$  denote the two image axes in the pixel space.  $S_u$  and  $S_v$  are marginalized versions of  $S$  along  $u$  and  $v$  respectively.

#### 3.2. Designing Saliency Guidance

Warping guidance decides which image regions are warped (e.g., scaled) more than others. Since images are warped *in-place*, if some regions are expanded, others must be reduced in size (Figure 4). For the warping mechanism considered [25, 36, 37], this requires designing a saliency function  $S$ . We investigate three saliency functions, based on two approximate guidances proposed in previous work [9, 36, 37] and one that we propose in this work.

**Approximate Saliency Guidance:** The Geometric Prior [9] assumes that a dominant vanishing point exists in the distant scene, and designs a saliency map to exploit this property and oversample objects that appear small. But this prior tries to warp the entire scene that is farther away and



the objects themselves may not be oversampled sufficiently to overcome size bias (Figure 4).

The Static Prior [36, 37] assumes that training set statistics will remain valid at test time, which is often not the case in domain adaptation due to domain shift and label unavailability. This incorrect assumption leads to the creation of a saliency map targeting average object locations, which may not accurately represent specific target images where objects deviate from these averages (Figure 4). Moreover, warping during the test phase, after adaptation, increases inference latency and is less effective due to the unknown scale distribution of the target domain (See Section 5.4 for ablation). Essentially, these saliency approaches do not utilize actual object labels and fail to concentrate on oversampling the objects, a strategy that would significantly benefit the shifting of the object scale distribution.

**Instance-level Saliency Guidance.** We propose Instance-level Saliency Guidance which explicitly shifts the object scale distribution by leveraging ground truth labels (Figure 4). During training, source image  $x_a$  has corresponding labels  $y_a$  available. For simplicity, we assume the labels are bounding boxes.

To shift the object scale distribution, we oversample image regions corresponding to every object instance. Following [1, 36], we use kernel density estimation to model the bounding box saliency as a sum of Gaussians,

$$S = \sum_{(c_i, w_i, h_i) \in y_a} \mathcal{N} \left( c_i, s \begin{bmatrix} w_i & 0 \\ 0 & h_i \end{bmatrix} \right) \quad (5)$$

where  $c_i$ ,  $w_i$  and  $h_i$  represent the center, width, and height of the bounding box,  $\mathcal{N}(\mu, \Sigma)$  is the normal distribution and  $s$  is the saliency scale or bandwidth.

We propose an expansion factor  $f$  to decide the warping extent of all objects,

$$f = 2^{\max \left( \left\lfloor \log_2 \left( \sum_{\psi \in \Psi} \frac{\psi_i}{\psi_{i+1}} \right) \right\rfloor, 0 \right)} \quad (6)$$

where  $\Psi$  is the fraction of object size corresponding to an interval between size thresholds  $t_i$  and  $t_{i+1}$  (See Figure 1). In our case, we consider  $\Psi = \{\psi_{small}, \psi_{medium}, \psi_{large}\}$  to represent the percentage of the small, medium, and large objects in the dataset, defined by COCO [20] thresholds for object sizes in the image.

Saliency scale  $s$  and expansion factor  $f$  are inversely proportional, thus  $s = \frac{P}{f}$  where  $P$  is a constant. We clip  $S$  between of 0 and  $U$ , since negative saliency values lead to holes, and an upper bound  $U$  to discourage extreme warping.

When segmentation masks are available but not bounding boxes, we convert them to boxes, termed ‘‘from-seg’’

boxes. This conversion minimally impacts performance, as detailed in our ablations in Section 5.4 and Supplementary.

### 3.3. Warping for Domain Adaptation

We consider unsupervised domain adaptation, wherein source domain  $\mathcal{X}_a$  is available with labels, i.e. dataset  $X_a = \{(x_a, y_a) \in \mathcal{X}_a\}$  and target domain  $\mathcal{X}_b$  only consists of images,  $X_b = \{x_b \in \mathcal{X}_b\}$ .

**Domain Adaption Framework:** The standard framework comprises of two stages. First, a supervised pre-training stage where a model  $\hat{y}_a = F_\theta(x_a)$  is trained using supervised loss on source domain,  $\mathcal{L}_{sup}(y_a, F_\theta(x_a))$ . Second, in the unsupervised adaptation stage the model is adapted to target domain  $\mathcal{X}_b$  using dataset  $X_b$  through an additional unsupervised loss. Generally, a student  $F_{s,\phi}$  and teacher  $F_{t,\kappa}$  (initialized using  $F_\theta$ ) are trained jointly through self-training, by employing psuedo labels [12, 17]. While training the student, a supervised loss is used to preserve performance on the source domain  $\mathcal{X}_a$  in a supervised branch:

$$\mathcal{L}_{sup}(y_a, F_{s,\phi}(x_a)) + \lambda \mathcal{L}_{unsup}(F_{t,\kappa}(x_b), F_{s,\phi}(x_b)) \quad (7)$$

The teacher is updated as the exponential moving average (EMA) of the student.

#### Warping and Unwarping in the Domain Adaptation Framework:

The design decisions that guide our choices are: (a) Maximize transferability of features from supervised stage to unsupervised training stages. (b) Warping at test time after adaptation is likely to be suboptimal as the target domain’s scale distribution is unknown and can introduce latency. If the target distribution is known, the Instance-level guidance can be shifted analytically to match this distribution. Thus, our warping mechanism  $W_{\mathcal{T}}$  operates only where images from source domain are used, i.e. it is employed in the supervised pre-training stage and the student model in the unsupervised stage when source image is forwarded. We do experiment by warping target images too while employing Static [36, 37] and Geometric prior [9] saliency guidances (which do not use ground truth object labels to generate saliency), however, that reduces performance (See Table 8).

Consider the recognition model  $F$  as a combination of backbone  $B$  and prediction heads  $H$ , i.e.  $F(x) = H(B(x))$ . We warp the image and then unwarp the feature maps from backbone  $B$  respectively to compose,

$$F'(x_a) = H(W_{\tilde{\tau}^{-1}}(B(W_{\mathcal{T}}(x_a)))) \quad (8)$$

following [37] for a source image  $x_a$ . Thus, losses are modified for the supervised pre-training stage as,

$$\mathcal{L}_{sup}(y_a, F'_\theta(x_a)) \quad (9)$$

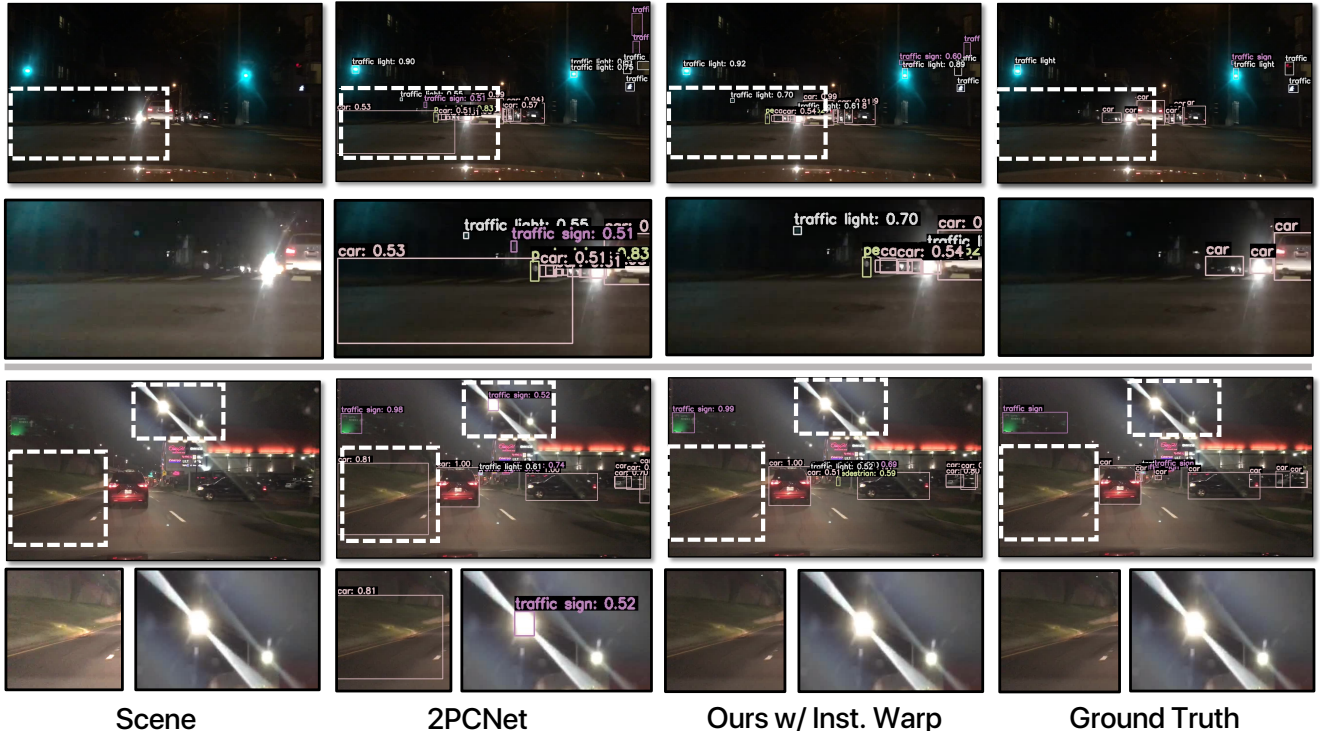


Figure 5. **Domain Adaptive Object Detection (BDD100K day  $\rightarrow$  night)**. Model trained with our method exhibits improved precision in distinguishing between road elements, accurately identifying cars and correctly detecting streetlights. Meanwhile, 2PCNet [17] appears to show a tendency to confuse these classes.

and for the unsupervised training stage as,

$$\mathcal{L}_{sup}(y_a, F'_{s,\phi}(x_a)) + \lambda \mathcal{L}_{unsup}(F_{t,\kappa}(x_b), F_{s,\phi}(x_b)) \quad (10)$$

For our experiments, we use DAFormer [12] and 2PCNet [17] as our baseline segmentation and detection domain adaption algorithms respectively. We do not make additional assumptions about the domain adaptation setup, and thus our method is agnostic to the task specification (segmentation or detection). Other domain adaption algorithms [6, 13, 14, 18, 48] are also applicable.

**Inference:** We employ the teacher model  $F_t$  during inference, and *do not require any image warping and feature unwarping at test time*. This is in contrast with image warping techniques proposed in the supervised setting [9, 36, 37], which incur overheads from test-time warping and assume additional information (like vanishing points [9]) to generate saliency maps at test time.

**Supervised Setting:** Our training method can also be applied in supervised learning scenario by following the supervised pre-training steps to train a model  $F'$ . That is, omitting the unsupervised training stage completely and only performing supervised pre-training stage – then removing the warping and unwarping layers completely from the trained model. This is unlike prior work [8, 25, 36, 37]

which advocates warping at test time too. Model performance improves significantly on target domain  $\mathcal{X}_b$  *without performing adaptation* (See Table 5). For Source Domain Results, see Supplementary Section C.

#### 4. Experimental Methodology and Datasets

We implement our source domain warping technique alongside a baseline domain adaptation algorithm, ensuring fair comparisons by using the same model, datasets, training schedules, hyperparameters, and random seeds.

**Object Detection:** Following the recent and popular domain adaptation strategy 2PCNet [17] (2023), we use Faster R-CNN [27] with ResNet-50 [10] adhering to their training hyperparameters and protocols. While 2PCNet [17] solely focuses on Day-to-Night adaptation, our method spans various adaptation scenarios. For scenarios other than day-to-night adaptation, we exclude the NightAug augmentation proposed in [17] for both the baseline and our method.

**Semantic Segmentation:** Aligning with the recent and popular domain adaptation strategy DAFormer [12] (2022), we employ the same SegFormer [44] head and MiT-B5 [44] backbone, and follow their training hyperparameters, protocols, and seed for fair comparison. While DAFormer [12] shows results on Sim2Real Gap which is not a focus of our

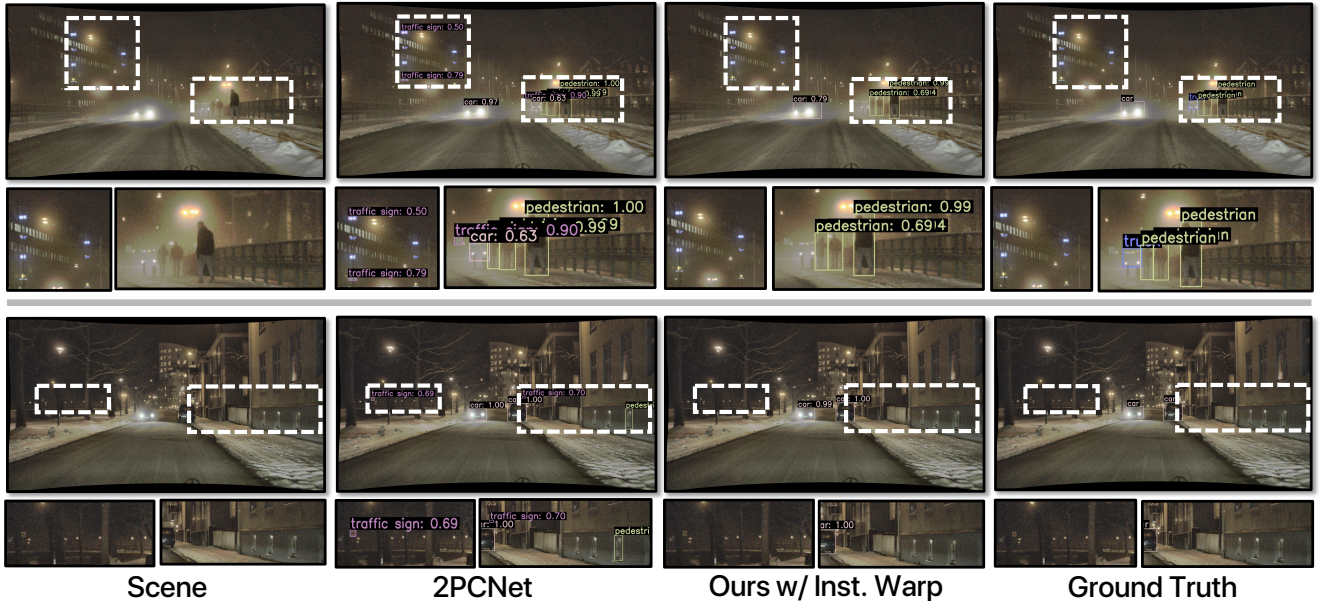


Figure 6. **Domain Adaptive Object Detection (BDD100K Clear → DENSE Foggy)**. Our method identifies streetlights and vehicles, which 2PCNet mislabels as traffic signs. Our method ignores windows, which 2PCNet misclassifies as pedestrians.

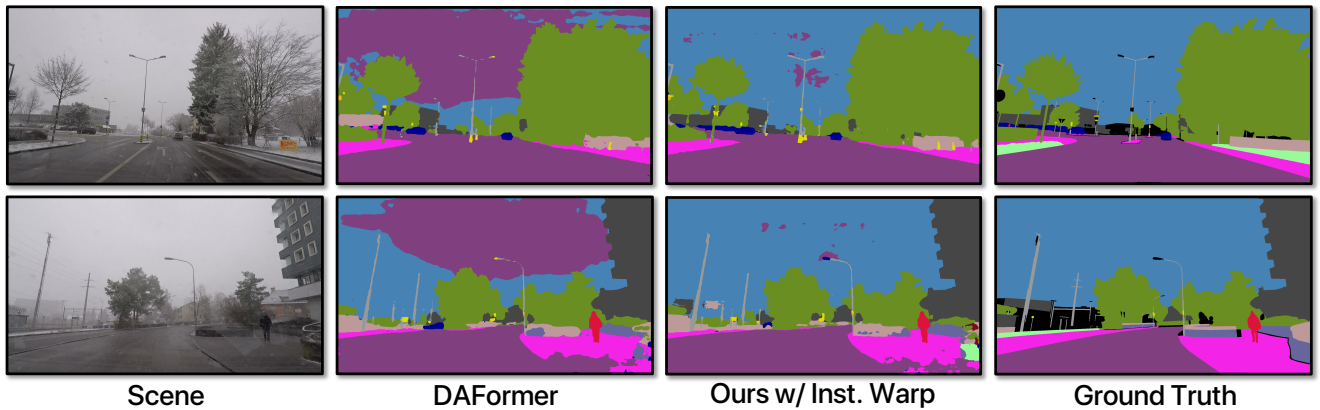


Figure 7. **Domain Adaptive Semantic Segmentation (Cityscapes → ACDC)**. Our warping significantly improved recognition of background elements like the sky, sidewalks, and buildings, as well as foreground objects such as traffic lights and traffic signs, indicating enhanced scene understanding ability.

work, results and discussion are available in Supplementary Section A. Extensions of DAFormer, including HRDA [13] and MIC [14], also benefits from our methodology, detailed in the Appendix B

#### 4.1. Datasets

**BDD100K** [47] features 100,000 images with a resolution of 1280x720 for object detection and segmentation, covering various weather conditions and times of day. It includes 10 categories for annotation.

**Cityscapes** [4] provides 5,000 images of urban road scenes at a resolution of 2048x1024 with clear weather for seman-

tic segmentation, with 19 categories.

**DENSE** [2] provides 12,997 images at a resolution of 1920x1024, capturing diverse weather conditions such as heavy fog and heavy snow.

**ACDC** [32] is designed for adverse conditions (fog and snow), including 1,600 images at 2048x1024 for segmentation across 19 categories.

**DarkZurich** [30] is tailored for low-light conditions, offering 2,416 unlabeled nighttime images and 151 labeled twilight images for segmentation, with a resolution of 1920x1080, and a focus on urban settings.



Table 1. **Adverse Weather: BDD100K Clear → DENSE Foggy.** Our method achieves notable improvements in **+6.1** mAP, **+6.1** mAP50, **+9.6** mAP75 and **+9.7** mAPI over 2PCNet. Instance Warping guidance is superior to the other priors.

Method	mAP	mAP50	mAP75	mAPs	mAPm	mAPI	person	car	truck	bike
2PCNet	27.0	45.0	30.1	0.0	15.4	35.5	87.5	72.5	19.1	0.9
+ Ours w/ Sta. Prior	28.6	48.5	31.7	0.0	<b>19.6</b>	34.0	<b>88.1</b>	72.5	25.6	<b>7.7</b>
+ Ours w/ Geo. Prior	27.1	45.8	29.5	0.0	15.2	37.5	86.5	<b>75.4</b>	21.0	0.4
+ Ours w/ Inst. Warp	<b>33.1</b>	<b>51.1</b>	<b>39.7</b>	0.0	14.5	<b>45.2</b>	85.8	66.3	<b>50.0</b>	2.2

Table 2. **Adverse Weather: BDD100K (Clear → Rainy) Object Detection.** Tested on BDD100k Rainy Val. Our method improves 2PCNet [17] (overall and per category) by **+3.0** mAP50. Instance-level performs best on mAP and mAP50 overall.

Method	mAP	mAP50	mAP75	mAPs	mAPm	mAPI	person	rider	car	truck	bus	motor cycle	bike	traffic light	traffic sign
2PCNet	25.8	48.4	24.4	10.9	34.1	49.0	56.3	40.4	77.0	57.2	55.9	36.8	36.8	55.6	68.1
+ Ours w/ Sta. Prior	26.8	50.6	<b>24.9</b>	11.4	35.9	49.6	<b>57.4</b>	42.5	77.4	<b>60.1</b>	59.5	44.8	39.4	55.7	68.9
+ Ours w/ Geo. Prior	26.9	49.9	24.5	<b>11.8</b>	35.6	<b>50.1</b>	56.1	44.6	<b>77.5</b>	58.0	58.6	33.3	<b>45.8</b>	<b>55.8</b>	<b>69.5</b>
+ Ours w/ Inst. Warp	<b>27.1</b>	<b>51.4</b>	24.6	11.0	<b>36.7</b>	49.0	57.2	<b>46.6</b>	<b>77.5</b>	59.8	<b>60.9</b>	<b>46.3</b>	42.2	54.9	68.3

Table 3. **Bad Lighting: BDD100K (Day → Night) Object Detection.** Tested on BDD100k Night Val. Our method improves state-of-the-art 2PCNet [17] (overall and per category) by **+3.7** mAP50. Geometric and Instance-level priors perform similarly overall with instance-level improving more categories.

Method	mAP	mAP50	mAP75	mAPs	mAPm	mAPI	person	rider	car	truck	bus	motor cycle	bike	traffic light	traffic sign
2PCNet	23.5	46.4	21.1	9.5	26.0	43.3	54.4	30.8	73.1	53.8	55.2	37.5	44.5	49.4	65.2
+ Ours w/ Sta. Prior	25.3	49.4	22.4	10.3	27.4	45.1	58.2	39.3	75.0	53.6	54.5	41.4	49.6	<b>52.9</b>	<b>69.6</b>
+ Ours w/ Geo. Prior	<b>25.6</b>	49.7	<b>22.9</b>	<b>10.0</b>	<b>27.7</b>	45.7	58.8	41.8	75.0	<b>55.8</b>	55.2	40.8	49.3	50.5	69.4
+ Ours w/ Inst. Warp	<b>25.6</b>	<b>50.1</b>	22.6	9.8	27.6	<b>46.6</b>	<b>58.9</b>	<b>42.7</b>	<b>75.1</b>	55.0	<b>55.5</b>	<b>42.6</b>	<b>50.1</b>	51.9	69.0

Table 4. **Changing Geography: BDD100K Clear → ACDC Object Detection.** Tested on ACDC Val. Our method improves 2PCNet [17] (overall and per category) by **+1.7** mAP50. Instance-level is superior to the other priors.

Method	mAP	mAP50	mAP75	mAPs	mAPm	mAPI	person	rider	car	truck	bus	motor cycle	bike
2PCNet	16.6	30.8	14.9	6.0	24.8	26.6	41.0	20.0	77.0	41.8	17.1	29.9	19.3
+ Ours w/ Sta. Prior	17.3	31.0	16.7	6.2	25.9	29.5	42.2	<b>20.9</b>	76.7	40.5	<b>21.7</b>	24.4	21.8
+ Ours w/ Geo. Prior	16.6	30.3	15.4	5.2	25.1	28.7	42.3	19.2	75.0	39.5	18.1	<b>26.7</b>	21.3
+ Ours w/ Inst. Warp	<b>17.9</b>	<b>32.1</b>	<b>18.2</b>	<b>6.8</b>	<b>26.7</b>	<b>32.1</b>	<b>45.7</b>	20.6	<b>77.6</b>	<b>43.2</b>	20.8	<b>26.7</b>	<b>22.2</b>

## 5. Experiments

### 5.1. Domain Adaptive Object Detection

Tables 1, 2, 3 and 4 show improvements of our method over state-of-the-art 2PCNet [17] across lighting, weather and geographic adaptations respectively. Moreover, our instance-level saliency guidance always improves over approximate saliency guidance [9, 36]. Note that 2PCNet [17] focused solely on day → night adaptation with its NightAug augmentation, which was only used in the BDD100K day → night experiment (Table 3) and omitted for others. Our method to address scale bias is more general in comparison.

Figures 5 and 6 shows examples where 2PCNet [17] mistakes parts of the road for cars and street lights for traffic

lights. In contrast, our method accurately detects these elements in difficult lighting and weather conditions.

### 5.2. Domain Adaptive Semantic Segmentation

To demonstrate our method is task agnostic, we incorporate it within domain adaptive semantic segmentation using the popular DAFormer [12] algorithm. The resulting approach shows significant improvement on both Val and Test Splits of the ACDC dataset (Table 5). Here, saliency guidance choice matters: our instance-level image saliency guidance outperforms Static Prior [36] and Geometric Prior [9]. Being agnostic to the DA algorithm, our method also boosts DAFormer extensions like HRDA [13] and MIC [14] (See Supplementary Section B). These extensions mitigate scale bias to some extent but add significant training memory

Table 5. **Cityscapes** → **ACDC Semantic Segmentation**. Tested on ACDC Val and Test-splits. Our method is superior, with or without Adaptation, implying better generalization of backbone and improves DAFormer by **+6.3** mIoU on Test-split.

Method	mIoU	road	side walk	building	wall	fence	pole	traffic light	traffic sign	vegetation	terrain	sky	person	rider	car	truck	bus	train	motor cycle	bike
<b>ACDC Val Split: After Supervised Pre-Training</b>																				
DAFormer [12]	55.8	77.6	<b>57.4</b>	77.9	39.4	30.4	48.3	54.5	<b>46.4</b>	70.0	<b>37.9</b>	72.2	52.6	32.0	81.4	72.7	73.7	70.4	37.6	27.3
+ Ours w/ Sta.	55.8	77.5	55.8	76.7	<b>39.8</b>	28.7	48.6	56.0	43.9	69.0	37.5	73.0	<b>53.6</b>	<b>32.9</b>	81.1	71.8	72.6	<b>82.5</b>	36.0	22.8
+ Ours w/ Geo.	55.7	<b>80.4</b>	57.3	<b>78.3</b>	37.7	28.4	48.2	54.4	44.8	<b>70.3</b>	37.4	75.1	52.8	30.5	80.7	75.6	72.8	65.8	38.9	29.8
+ Ours w/ Inst.	<b>56.8</b>	80.2	48.3	76.0	35.0	<b>31.6</b>	<b>48.6</b>	<b>58.2</b>	45.3	69.4	36.9	<b>77.2</b>	53.2	26.2	<b>82.0</b>	<b>77.6</b>	<b>80.0</b>	69.4	<b>39.7</b>	<b>43.7</b>
<b>ACDC Val Split: After Unsupervised Domain Adaptation</b>																				
DAFormer [12]	57.6	72.7	57.5	<b>80.1</b>	42.5	38.0	50.9	45.1	50.0	71.1	38.5	67.0	56.0	29.9	81.8	76.6	78.9	79.9	40.8	36.7
+ Ours w/ Sta.	59.1	73.8	56.8	79.1	<b>45.2</b>	39.6	50.0	48.3	49.4	71.0	<b>39.3</b>	68.6	55.8	<b>36.9</b>	82.1	73.2	81.3	<b>88.7</b>	37.1	<b>47.4</b>
+ Ours w/ Geo.	58.4	76.4	<b>57.6</b>	79.9	42.2	39.0	51.7	46.4	49.5	72.0	39.0	71.1	56.5	30.4	82.7	79.3	79.1	69.8	41.5	44.7
+ Ours w/ Inst.	<b>61.8</b>	<b>82.9</b>	56.1	79.8	44.6	<b>40.3</b>	<b>52.7</b>	<b>60.8</b>	<b>52.5</b>	<b>72.0</b>	38.4	<b>78.0</b>	<b>56.6</b>	30.5	<b>84.9</b>	<b>80.2</b>	<b>86.9</b>	86.4	<b>44.5</b>	45.8
<b>ACDC Test Split Results</b>																				
ADVENT [40]	32.7	<b>72.9</b>	14.3	40.5	16.6	21.2	9.3	17.4	21.2	63.8	23.8	18.3	32.6	19.5	69.5	36.2	34.5	46.2	26.9	36.1
MGCDA [30]	48.7	73.4	28.7	69.9	19.3	26.3	36.8	<b>53.0</b>	53.3	<b>75.4</b>	32.0	84.6	51.0	26.1	77.6	43.2	45.9	53.9	32.7	41.5
DANNet [43]	50.0	<b>84.3</b>	<b>54.2</b>	77.6	38.0	30.0	18.9	41.6	35.2	71.3	39.4	<b>86.6</b>	48.7	29.2	76.2	41.6	43.0	58.6	32.6	43.9
DAFormer [12]	55.4	58.4	51.3	84.0	42.7	35.1	<b>50.7</b>	30.0	57.0	74.8	52.8	51.3	58.3	<b>32.6</b>	82.7	58.3	54.9	82.4	44.1	50.7
+ Ours w/ Inst.	<b>61.7</b>	83.0	53.2	<b>85.5</b>	<b>47.4</b>	<b>38.3</b>	46.0	51.4	<b>57.8</b>	73.9	<b>56.2</b>	82.1	<b>61.3</b>	32.3	<b>85.5</b>	<b>69.0</b>	<b>68.9</b>	<b>82.5</b>	<b>46.7</b>	<b>52.0</b>

Table 6. **Cityscapes** → **DarkZurich Semantic Segmentation**. Tested on DarkZurich Val and Test. Our method is superior, with or without Adaptation, implying better generalization of backbone and improves DAFormer by **+3.3** mIoU on Val-split.

Method	mIoU	road	side walk	building	wall	fence	pole	traffic light	traffic sign	vegetation	terrain	sky	person	rider	car	truck	bus	train	motor cycle	bike
<b>DarkZurich Val Split: After Supervised Pre-Training</b>																				
DAFormer	30.0	90.7	52.7	45.5	18.4	39.0	38.4	27.5	18.3	<b>59.0</b>	26.5	11.1	20.4	21.1	58.6	-	-	-	22.1	20.0
+ Ours w/ Sta.	32.7	91.8	57.2	47.3	19.3	<b>46.2</b>	<b>40.1</b>	21.0	18.2	53.5	<b>31.9</b>	6.4	20.6	18.6	<b>64.1</b>	-	-	-	25.0	26.4
+ Ours w/ Geo.	30.2	89.9	50.5	45.9	20.5	36.8	39.1	21.0	<b>19.8</b>	54.7	28.4	7.9	19.0	<b>31.1</b>	58.4	-	-	-	18.1	33.4
+ Ours w/ Inst.	<b>34.0</b>	<b>91.9</b>	<b>59.4</b>	<b>49.3</b>	<b>27.7</b>	39.2	39.4	<b>27.6</b>	15.8	55.1	29.9	<b>11.4</b>	<b>20.7</b>	9.2	61.9	-	-	-	<b>27.9</b>	<b>44.7</b>
<b>DarkZurich Val Split: After Unsupervised Domain Adaptation</b>																				
DAFormer	33.8	92.0	66.7	47.3	25.9	50.8	38.0	24.6	19.4	<b>62.2</b>	31.9	17.9	20.4	<b>28.4</b>	61.7	-	-	-	21.0	34.3
+ Ours w/ Sta.	33.8	<b>93.3</b>	68.5	50.0	28.4	<b>54.3</b>	<b>41.7</b>	19.9	22.7	54.0	<b>41.5</b>	14.1	22.9	7.2	62.6	-	-	-	<b>24.6</b>	<b>36.8</b>
+ Ours w/ Geo.	33.3	84.3	60.3	<b>60.2</b>	23.9	49.4	38.7	12.7	<b>25.0</b>	52.0	39.5	20.8	<b>37.1</b>	16.2	64.6	-	-	-	21.1	27.8
+ Ours w/ Inst.	<b>37.1</b>	88.7	<b>70.9</b>	60.1	<b>42.1</b>	49.6	39.8	<b>47.9</b>	21.5	49.8	35.7	<b>25.4</b>	23.8	25.9	<b>66.8</b>	-	-	-	24.3	32.4
<b>DarkZurich Test Split Results</b>																				
ADVENT [40]	29.7	85.8	37.9	55.5	27.7	14.5	23.1	14.0	21.1	32.1	8.7	2.0	39.9	16.6	64.0	13.8	0.0	58.8	28.5	20.7
MGCDA [30]	42.5	80.3	49.3	66.2	7.8	11.0	41.4	38.9	39.0	64.1	18.0	55.8	52.1	<b>53.5</b>	74.7	<b>66.0</b>	0.0	37.5	29.1	22.7
DANNet [43]	44.3	90.0	54.0	<b>74.8</b>	41.0	21.1	25.0	26.8	30.2	<b>72.0</b>	26.2	<b>84.0</b>	47.0	33.9	68.2	19.0	0.3	66.4	38.3	23.6
DAFormer [12]	53.8	93.5	65.5	73.3	39.4	19.2	<b>53.3</b>	44.1	44.0	59.5	<b>34.5</b>	66.6	53.4	52.7	<b>82.1</b>	52.7	9.5	89.3	50.5	38.5
+ Ours w/ Inst.	<b>54.4</b>	<b>94.2</b>	<b>68.1</b>	72.6	<b>43.2</b>	<b>23.6</b>	51.0	<b>48.1</b>	<b>48.5</b>	60.6	33.6	54.8	<b>55.5</b>	49.0	79.8	51.1	<b>13.2</b>	<b>90.2</b>	<b>53.2</b>	<b>43.4</b>

(+5GB) and inference latency (+800 ms on RTX 4090 GPU), whereas our approach requires negligible additional training memory (+0.04 GB) and adds no additional inference latency.

Table 5 also shows our method’s superiority across scenarios, with or without unsupervised domain adaptation. This suggests that the learned backbone features due to our method generalize better to unseen domains. Additionally, Figure 7 illustrates superior performance of our method in identifying both background elements (e.g., sky, sidewalks, buildings) and foreground objects (e.g., traffic lights and traffic signs).

### 5.3. Visual Diagnosis of Learned Models

In Section 5.2, we noted that the learned backbone feature of our method generalize better. To corroborate this claim, we employed GradCAM [33] visualizations, showcasing ResNet features from detectors trained on BDD100K [47] in Figure 8. The heatmap for models trained with 2PCNet without warping reveals a dispersed focus across the im-

age, indicating a lack of precision. The choice of saliency guidance plays a critical role: warping guided by Geometric Prior [9] results in less focus on the target (e.g., cars) and unnecessary background emphasis. Conversely, our instance-level saliency guidance achieves a focused heatmap on relevant objects, minimizing irrelevant activations.

### 5.4. Ablation Study

For all ablation studies, we utilize the Cityscape → ACDC domain adaptive semantic segmentation task.

**Saliency Product  $P$  and Upperbound  $U$ .** Varying  $P$  and  $U$  shows optimal performance at  $P = 2^8$  and  $U = 1.0$ , according to quantitative scores in Table 7a. Hence,  $P = 2^8$  and  $U = 1.0$  are adopted for all major experiments.

**Warping on Source vs. Target.** Given the necessity of ground truth labels for our instance-level saliency guidance, warping in the target domain for unsupervised domain adaptation is infeasible. Nevertheless, as shown in Table 8 warping source domain images with our saliency guidance

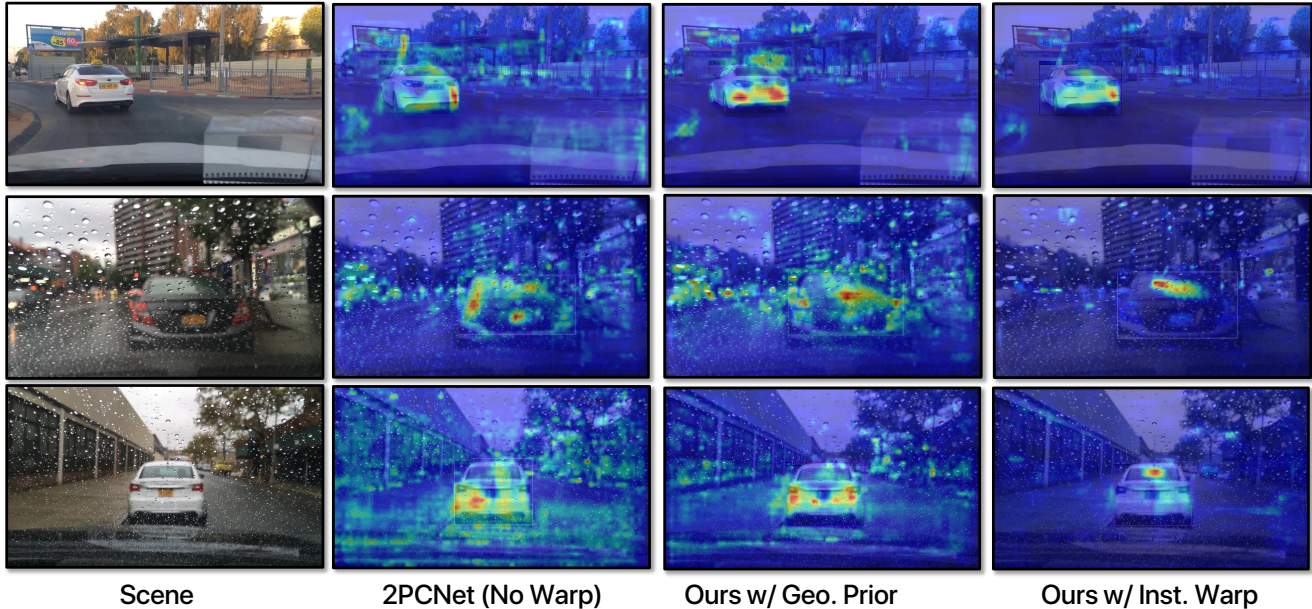


Figure 8. **Grad-Cam [33] Visualization of the Last Layer Feature of the Learnt ResNet-50 Backbone.** Learned features due to our method has a higher degree of focus, implying better learned features and scene comprehension ability.

Table 7. **Ablations:** (a) Studying the impact of hyperparameters  $P$  and  $U$ , same parameters used for all other experiments. (b) Studying the impact of balancing the scale distribution by undersampling the dataset.

(a) Saliency Product  $P$  and Upperbound  $U$ . Trained on Cityscapes  $\rightarrow$  ACDC and tested on ACDC Val. While  $P = 2^8$  and  $U = 1.00$  are optimal, our model requires minimal engineering due to the small mIoU range (1.7%).

Parameters	aAcc	mIoU	mAcc
$P=2^7, U=1.00$	84.7	60.1	73.2
$P=2^9, U=1.00$	84.2	61.4	<b>74.1</b>
$P=2^8, U=0.50$	85.2	60.1	72.5
$P=2^8, U=0.75$	82.4	60.3	73.1
$P=2^8, U=1.00$	<b>85.3</b>	<b>61.8</b>	73.8

(b) Balanced Undersampling Strategy. Trained on Cityscapes and tested on Cityscapes Val using Supervised strategy in Section 3.3. Undersampling images to address scale bias hinders segmentation.

Sample	Percent	Method	aAcc	mIoU	mAcc
Uniform	25%	SegFormer	95.0	71.0	79.1
		Ours	95.1	71.9	80.0
	50%	SegFormer	95.3	73.6	81.4
		Ours	95.5	74.4	82.1
None	100%	SegFormer	95.6	75.3	82.9
		Ours	<b>95.9</b>	<b>76.8</b>	<b>84.2</b>

surpasses performance using approximated saliency [9, 36] with both source and target domain warping.

**Warping with From-Seg vs. Groundtruth bboxes.** For object detection, we utilize ground truth bounding boxes for saliency guidance. However, semantic segmentation tasks often lack this data, leading us to use bounding boxes computed from segmentations, “from-seg” for short. Results indicate superior performance with ground truth boxes, but “from-seg” boxes are a close second, highlighting their effectiveness when ground truth is unavailable (Table 8).

**Distribution Balancing by Undersampling.** We analyzed undersampling strategies that balance the percentages of small, medium, and large objects, aiming to create a more uniform distribution that mitigates scale bias. As shown in Table 7b, our experiments applying 25% and 50% of undersampling to the Cityscapes dataset indicates that mod-

els trained on these “uniform” subsets perform worse than those trained on the complete dataset, highlighting the challenges of addressing scale bias through simple subsampling.

## 6. Limitations and Conclusion

In this work, we address scale bias with attentional processing, using saliency-guided image warping that integrates seamlessly into any unsupervised domain adaptation method. Leveraging scale statistics from the source dataset and ground truth labels, our approach effectively navigates challenges in lighting, weather, and geographic differences. Extensive experiments demonstrate the effectiveness of our warping method and instance-level saliency guidance. Importantly, our approach adds no inference latency. Depending on the available information (e.g., vanishing point, target statistics), other priors could be used with our approach,



Table 8. **Ablation: Warping (source/target domain) and Bounding Box Type (from-seg/ground truth).** Trained on Cityscapes → ACDC. Tested on ACDC Val. Using ground truth bounding boxes are better than using bounding boxes derived from semantic segmentation. In case of Static prior and Geometric prior, we can apply warping during target adaptation and testing as they do not rely on ground truth. In case of Inst., *target and test warping is impossible as ground truth boxes are unavailable in the target domain*, as per the definition of unsupervised domain adaptation.

Method	Warp	Bboxes	aAcc	mIoU	mAcc
DAFormer	-	-	81.9	57.6	70.6
+ Ours w/ Sta. Prior	src & tgt & test	-	82.5	55.3	68.3
	src & tgt	-	83.8	57.4	69.6
	src	-	82.3	59.1	73.3
+ Ours w/ Geo. Prior	src & tgt & test	-	82.2	57.7	71.6
	src & tgt	-	81.9	56.5	70.9
	src	-	83.2	58.4	70.9
+ Ours w/ Inst. (tgt & test inapplicable)	src	from-seg	84.0	60.1	73.5
	src	gt	<b>85.3</b>	<b>61.8</b>	<b>73.8</b>

showing improvement over baselines, albeit to a lesser extent.

One limitation of our method arises in densely populated scenes (e.g., New York’s Times Square), where the limited background space challenges the expansion and contraction capabilities of our warping. Besides, our approach is less effective on certain synthetic datasets, such as Synthia [29], which do not exhibit realistic scale bias. However, our approach proves effective on other synthetic datasets like GTA5 [28], a role-playing game dataset featuring city driving components with realistic traffic and exhibiting realistic scale biases.

**Societal Impact.** While our method demonstrates improved perception on publicly available night and adverse weather driving datasets, extensive testing is required before real-world deployment on self-driving vehicles.

**Acknowledgment.** This work was supported in parts by a sponsored research contract from General Motors Research-Israel, NSF grant CNS-2038612, and DOT RITA Mobility-21 Grant 69A3551747111.

## References

- [1] Hui Bi, Hui Tang, Guanyu Yang, Huazhong Shu, and Jean-Louis Dillenseger. Accurate image segmentation using gaussian mixture model with saliency map. *Pattern Analysis and Applications*, 2018. 5
- [2] Mario Bijelic, Tobias Gruber, Fahim Mannan, Florian Kraus, Werner Ritter, Klaus Dietmayer, and Felix Heide. Seeing through fog without seeing fog: Deep multimodal sensor fusion in unseen adverse weather. In *CVPR*, 2020. 7
- [3] Ting-Wu Chin, Ruizhou Ding, and Diana Marculescu. Adascale: Towards real-time video object detection using adaptive scaling. *MLSys*, 2019. 3
- [4] Marius Cordts, Mohamed Omran, Sebastian Ramos, Timo Rehfeld, Markus Enzweiler, Rodrigo Benenson, Uwe Franke, Stefan Roth, and Bernt Schiele. The cityscapes dataset for semantic urban scene understanding. In *CVPR*, 2016. 7, 14
- [5] Navneet Dalal and Bill Triggs. Histograms of oriented gradients for human detection. In *CVPR*, 2005. 3
- [6] Jinhong Deng, Wen Li, Yuhua Chen, and Lixin Duan. Unbiased mean teacher for cross-domain object detection. In *CVPR*, 2021. 3, 6
- [7] Babak Ehteshami Bejnordi, Amirhossein Habibian, Fatih Porikli, and Amir Ghodrati. Salisa: Saliency-based input sampling for efficient video object detection. In *ECCV*, 2022. 2, 4
- [8] Anurag Ghosh, Vaibhav Balloli, Akshay Nambi, Aditya Singh, and Tanuja Ganu. Chanakya: Learning runtime decisions for adaptive real-time perception. In *NeurIPS*, 2023. 3, 6
- [9] Anurag Ghosh, N Dinesh Reddy, Christoph Mertz, and Srini-vasa G Narasimhan. Learned two-plane perspective prior based image resampling for efficient object detection. In *CVPR*, 2023. 2, 3, 4, 5, 6, 8, 9, 10
- [10] Kaiming He, Xiangyu Zhang, Shaoqing Ren, and Jian Sun. Deep residual learning for image recognition. In *CVPR*, 2016. 2, 3, 6
- [11] Mengzhe He, Yali Wang, Jiayi Wu, Yiru Wang, Hanqing Li, Bo Li, Weihao Gan, Wei Wu, and Yu Qiao. Cross domain object detection by target-perceived dual branch distillation. In *CVPR*, 2022. 3
- [12] Lukas Hoyer, Dengxin Dai, and Luc Van Gool. Daformer: Improving network architectures and training strategies for domain-adaptive semantic segmentation. In *CVPR*, 2022. 3, 5, 6, 8, 9, 13, 14, 15, 16
- [13] Lukas Hoyer, Dengxin Dai, and Luc Van Gool. HRDA: Context-aware high-resolution domain-adaptive semantic segmentation. In *ECCV*, 2022. 2, 3, 6, 7, 8, 13, 15, 16
- [14] Lukas Hoyer, Dengxin Dai, Haoran Wang, and Luc Van Gool. MIC: Masked image consistency for context-enhanced domain adaptation. In *CVPR*, 2023. 3, 6, 7, 8, 13, 16
- [15] Jonathan Huang, Vivek Rathod, Chen Sun, Menglong Zhu, Anoop Korattikara, Alireza Fathi, Ian Fischer, Zbigniew Wojna, Yang Song, Sergio Guadarrama, et al. Speed/accuracy

- trade-offs for modern convolutional object detectors. In *CVPR*, 2017. 3
- [16] Max Jaderberg, Karen Simonyan, Andrew Zisserman, et al. Spatial transformer networks. *NeurIPS*, 2015. 3, 4
- [17] Mikhail Kennerley, Jian-Gang Wang, Bharadwaj Veeravalli, and Robby T Tan. 2pcnet: Two-phase consistency training for day-to-night unsupervised domain adaptive object detection. In *CVPR*, 2023. 3, 5, 6, 8, 13, 14, 18
- [18] Yu-Jhe Li, Xiaoliang Dai, Chih-Yao Ma, Yen-Cheng Liu, Kan Chen, Bichen Wu, Zijian He, Kris Kitani, and Peter Vajda. Cross-domain adaptive teacher for object detection. In *CVPR*, 2022. 3, 6
- [19] Di Lin, Yuanfeng Ji, Dani Lischinski, Daniel Cohen-Or, and Hui Huang. Multi-scale context intertwining for semantic segmentation. In *ECCV*, 2018. 1
- [20] Tsung-Yi Lin, Michael Maire, Serge Belongie, James Hays, Pietro Perona, Deva Ramanan, Piotr Dollár, and C Lawrence Zitnick. Microsoft coco: Common objects in context. In *ECCV*, 2014. 5
- [21] Tsung-Yi Lin, Piotr Dollár, Ross Girshick, Kaiming He, Bharath Hariharan, and Serge Belongie. Feature pyramid networks for object detection. In *CVPR*, 2017. 2, 3
- [22] Shu Liu, Lu Qi, Haifang Qin, Jianping Shi, and Jiaya Jia. Path aggregation network for instance segmentation. In *CVPR*, 2018. 3
- [23] David G Lowe. Distinctive image features from scale-invariant keypoints. *IJCV*, 2004. 2, 3
- [24] Ke Mei, Chuang Zhu, Jiaqi Zou, and Shanghang Zhang. Instance adaptive self-training for unsupervised domain adaptation. In *ECCV*, 2020. 3
- [25] Adria Recasens, Petr Kellnhofer, Simon Stent, Wojciech Matusik, and Antonio Torralba. Learning to zoom: a saliency-based sampling layer for neural networks. In *ECCV*, 2018. 2, 3, 4, 6
- [26] Joseph Redmon and Ali Farhadi. Yolov3: An incremental improvement. *arXiv preprint arXiv:1804.02767*, 2018. 3
- [27] Shaoqing Ren, Kaiming He, Ross Girshick, and Jian Sun. Faster r-cnn: Towards real-time object detection with region proposal networks. *NeurIPS*, 2015. 3, 6
- [28] Stephan R Richter, Vibhav Vineet, Stefan Roth, and Vladlen Koltun. Playing for data: Ground truth from computer games. In *ECCV*, 2016. 11, 13, 14
- [29] German Ros, Laura Sellart, Joanna Materzynska, David Vazquez, and Antonio M Lopez. The synthia dataset: A large collection of synthetic images for semantic segmentation of urban scenes. In *CVPR*, 2016. 11, 13, 14
- [30] Christos Sakaridis, Dengxin Dai, and Luc Van Gool. Guided curriculum model adaptation and uncertainty-aware evaluation for semantic nighttime image segmentation. In *ICCV*, 2019. 7, 9
- [31] Christos Sakaridis, Dengxin Dai, and Luc Van Gool. Map-guided curriculum domain adaptation and uncertainty-aware evaluation for semantic nighttime image segmentation. *TPAMI*, 2020. 3
- [32] Christos Sakaridis, Dengxin Dai, and Luc Van Gool. Acde: The adverse conditions dataset with correspondences for semantic driving scene understanding. In *ICCV*, 2021. 7, 14
- [33] Ramprasaath R Selvaraju, Michael Cogswell, Abhishek Das, Ramakrishna Vedantam, Devi Parikh, and Dhruv Batra. Grad-cam: Visual explanations from deep networks via gradient-based localization. In *ICCV*, 2017. 9, 10
- [34] Abhinav Shrivastava, Abhinav Gupta, and Ross Girshick. Training region-based object detectors with online hard example mining. In *CVPR*, 2016. 2, 3
- [35] Bharat Singh and Larry S Davis. An analysis of scale invariance in object detection snip. In *CVPR*, 2018. 1, 2, 3
- [36] Chittesh Thavamani, Mengtian Li, Nicolas Cebron, and Deva Ramanan. Fovea: Foveated image magnification for autonomous navigation. In *ICCV*, 2021. 2, 3, 4, 5, 6, 8, 10
- [37] Chittesh Thavamani, Mengtian Li, Francesco Ferroni, and Deva Ramanan. Learning to zoom and unzoom. In *CVPR*, 2023. 2, 3, 4, 5, 6
- [38] Wilhelm Truheden, Viktor Olsson, Juliano Pinto, and Lennart Svensson. Dacs: Domain adaptation via cross-domain mixed sampling. In *WACV*, 2021. 3, 14, 15
- [39] Yi-Hsuan Tsai, Wei-Chih Hung, Samuel Schuster, Kihyuk Sohn, Ming-Hsuan Yang, and Manmohan Chandraker. Learning to adapt structured output space for semantic segmentation. In *CVPR*, 2018. 3
- [40] Tuan-Hung Vu, Himalaya Jain, Maxime Bucher, Matthieu Cord, and Patrick Pérez. Advent: Adversarial entropy minimization for domain adaptation in semantic segmentation. In *CVPR*, 2019. 9
- [41] Qin Wang, Dengxin Dai, Lukas Hoyer, Luc Van Gool, and Olga Fink. Domain adaptive semantic segmentation with self-supervised depth estimation. In *ICCV*, 2021. 3, 14, 15
- [42] George Wolberg. *Digital image warping*. IEEE Computer Society Press Los Alamitos, CA, 1990. 3
- [43] Xinyi Wu, Zhenyao Wu, Hao Guo, Lili Ju, and Song Wang. Dattet: A one-stage domain adaptation network for unsupervised nighttime semantic segmentation. In *CVPR*, 2021. 3, 9
- [44] Enze Xie, Wenhai Wang, Zhiding Yu, Anima Anandkumar, Jose M Alvarez, and Ping Luo. Segformer: Simple and efficient design for semantic segmentation with transformers. *NeurIPS*, 2021. 6
- [45] Maoke Yang, Kun Yu, Chi Zhang, Zhiwei Li, and Kuiyuan Yang. Denseaspp for semantic segmentation in street scenes. In *CVPR*, 2018. 1, 3
- [46] Yanchao Yang and Stefano Soatto. Fda: Fourier domain adaptation for semantic segmentation. In *CVPR*, 2020. 3
- [47] Fisher Yu, Haofeng Chen, Xin Wang, Wenqi Xian, Yingying Chen, Fangchen Liu, Vashisht Madhavan, and Trevor Darrell. Bdd100k: A diverse driving dataset for heterogeneous multitask learning. In *CVPR*, 2020. 7, 9
- [48] Pan Zhang, Bo Zhang, Ting Zhang, Dong Chen, Yong Wang, and Fang Wen. Prototypical pseudo label denoising and target structure learning for domain adaptive semantic segmentation. In *CVPR*, 2021. 3, 6, 14, 15
- [49] Peng Zhou, Bingbing Ni, Cong Geng, Jianguo Hu, and Yi Xu. Scale-transferrable object detection. In *CVPR*, 2018. 1
- [50] Yang Zou, Zhiding Yu, BVK Kumar, and Jinsong Wang. Unsupervised domain adaptation for semantic segmentation via class-balanced self-training. In *ECCV*, 2018. 14, 15

## A. Synthetic to Real Domain Adaptation

Our proposed method addresses source scale biases that are present in natural scene datasets. *Synthetic To Real (Sim2Real) Domain Gap is not a focus of our work as a synthetic scene dataset may or may not exhibit the same bias.*

However, we do explore if our method improves performance on the Sim2Real Domain Gap by considering GTA [28] and Synthia [29] synthetic datasets. Table 9 and Table 10 show the results for GTA  $\rightarrow$  Cityscapes and Synthia  $\rightarrow$  Cityscapes domain adaptation respectively.

Our method improves GTA  $\rightarrow$  Cityscapes adaptation considerably, while improvement on Synthia  $\rightarrow$  Cityscapes adaptation is marginal, which corresponds to our intuition regarding both the source datasets (See Fig 9).

Grand Theft Auto 5 (GTA) is a role playing game with a city driving component along with realistic traffic, thus *GTA images are close to real driving scenes and hence exhibits similar scale biases.* Synthia, on the other hand, is a rendered dataset of a virtual city, and does not have realistic traffic simulation of dynamic objects like cars and people. Moreover, many images are not captured from a vehicle’s perspective. *Thus, images are not close to real driving scenes and do not exhibit scale bias.*

## B. Comparison with other Domain Adaptation Strategies

Domain adaptation extensions have been proposed on the DAFormer [12] training framework, such as HRDA [13] and MIC [14] which also show good performance.

**Differences from DAFormer.** HRDA [13] proposed a multi-scale high-resolution crop training strategy along with sliding window inference. MIC [14] proposed a masking consistency strategy for target domain images to improve spatial context.

HRDA [13] departs from DAFormer [12] by increasing training and inference image scales by a factor of 2 and performing sliding window inference (a test time scale augmentation). Training and inference computational costs significantly increase with HRDA’s strategy [13]. Correspondingly, our inference costs are same as DAFormer [12] (as we *do not* warp during test-time) while training time and memory consumption is marginally higher (See Table 11). Lastly, instance-level image warping is orthogonal to the aforementioned training strategies and can be used simultaneously with other training strategies.

**Evaluation Methodology.** Based on the above discussion, we apply HRDA’s and MIC’s strategy on DAFormer, but for a fair comparison, we perform training and inference *following DAFormer’s [12] training/testing image scales and evaluation paradigm.* The alternative comparison would be to train and evaluate on full-scale images for parity with

HRDA, however, we do not have a GPU with high memory availability (like NVIDIA Tesla A40 with 48 GB or Tesla A100 with 80 GB memory).

**Results.** Table 12 and 13 present results for Cityscapes  $\rightarrow$  DarkZurich and Cityscapes  $\rightarrow$  ACDC respectively. MIC (HRDA) corresponds to MIC and HRDA training strategies added to DAFormer. We compare with DAFormer and MIC (HRDA) with and without including our Instance-level image warping approach. We observe smaller improvements in conjunction with our method with MIC (HRDA) as HRDA uses multi-scale cropping strategies, which also attempts to alleviate scale bias to some extent.

As our instance-level image warping approach is orthogonal to other training strategies and can be used in plug-and-play manner, we studied the interaction of our method with MIC [14] and HRDA [13] individually (See Table 14).

We observed that our method when employed in conjunction with MIC and HRDA consistently improved performance, however, was not able to improve upon the scenario where our method is applied to DAFormer directly. Moreover, HRDA failed to improve upon DAFormer itself when trained on DAFormer’s training scale ( $1024 \times 512$ ) instead of full scale ( $2048 \times 1024$ ).

We concluded that high resolution training is necessary for HRDA as posited [13] and the strategy does not work at all image scales. Further, we observed HRDA performs two kinds of cropping – a HR-detail crop to better segment small object details and LR-context crop to adapt better to large objects. At DAFormer’s training scales, the cropped size of the detail crop would be very small and hurt performance. The advantage of our instance-level warping method is that it increases focus on small object details, thus we replaced detail crop with our instance level image warping. Removing detail crop from HRDA improved performance over DAFormer itself, and in conjunction with our method showed the best performance.

## C. Supervised Setting

In Section 3.2, we mentioned that source pre-training also improves performance in the supervised setting on the source domain itself. We show improvements in segmentation performance on Cityscapes, when applied to SegFormer model (base architecture of the DAFormer [12] training strategy), see Table 15. Please observe visual results of our method in Figure 10. We also show improvements in detection performance on BDD100K (Day) and BDD100 (Clear) when applied to Faster R-CNN (base architecture of 2PCNet [17] training strategy), see Table 16 and Table 17. BDD100K (Day) includes both clear and bad weather images taken during the day, while BDD100K (Clear) includes both day and night images taken in clear weather.



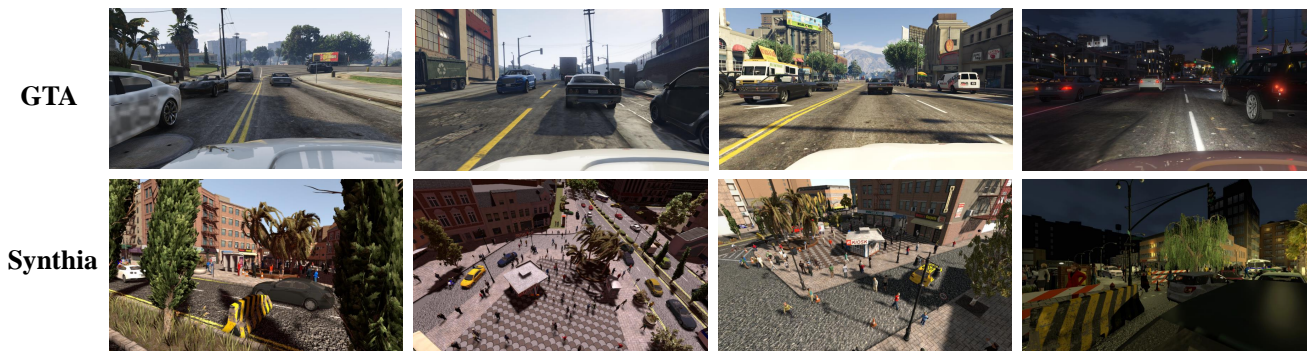


Figure 9. **Synthetic to Real Domain Adaptation.** GTA [28] consist of realistic scenes from vehicle’s perspective with realistic road traffic simulation, more closely reflecting object scale biases present in real-world driving scenes. In contrast, Synthia [29] consists of virtual world images that do not represent the scale biases of natural driving scenes.

Table 9. **Synthetic to Real Domain Adaptation: GTA  $\rightarrow$  Cityscapes Semantic Segmentation.** Tested on Cityscapes Val. We were unable to reproduce DAFormer’s [12] results averaged over 3 random seeds, hence we present results with seed=0 for both DAFormer [12] and our method (DAFormer with Instance-level Image Warping). *We do not target adaptation from synthetic datasets and Sim2Real Domain Gap, as synthetic datasets may not have a scale bias. However, GTA appears to have a scale bias like natural driving scenes.* This is due to realistic traffic simulation and all the captured imagery is from a vehicle’s perspective (See Figure 9). Our method shows improved performance on many individual categories.

Method	mIoU	road	side walk	building	wall	fence	pole	traffic light	traffic sign	vegetation	terrain	sky	person	rider	car	truck	bus	train	motor cycle	bike
CBST [50]	45.9	91.8	53.5	80.5	32.7	21.0	34.0	28.9	20.4	83.9	34.2	80.9	53.1	24.0	82.7	30.3	35.9	16.0	25.9	42.8
DACS [38]	52.1	89.9	39.7	87.9	30.7	39.5	38.5	46.4	52.8	88.0	44.0	88.8	67.2	35.8	84.5	45.7	50.2	0.0	27.3	34.0
CorDA [41]	56.6	94.7	63.1	87.6	30.7	40.6	40.2	47.8	51.6	87.6	47.0	89.7	66.7	35.9	90.2	48.9	57.5	0.0	39.8	56.0
ProDA [48]	57.5	87.8	56.0	79.7	46.3	44.8	45.6	53.5	53.5	88.6	45.2	82.1	70.7	39.2	88.8	45.5	59.4	1.0	48.9	56.4
DAFormer [12]	68.3	<b>95.7</b>	<b>70.2</b>	89.4	53.5	48.1	<b>49.6</b>	55.8	59.4	<b>89.9</b>	47.9	<b>92.5</b>	72.2	44.7	92.3	74.5	78.2	65.1	55.9	61.8
DAFormer (seed=0)	66.9	92.6	58.9	89.3	54.2	42.7	49.4	57.0	55.8	89.2	49.8	89.5	<b>72.7</b>	41.7	92.0	62.0	<b>82.8</b>	<b>71.3</b>	56.5	62.9
+ Ours	<b>68.5</b>	92.9	60.0	<b>89.8</b>	<b>55.9</b>	<b>51.5</b>	49.0	<b>57.2</b>	<b>62.2</b>	89.6	<b>50.2</b>	91.5	71.9	<b>44.8</b>	<b>93.0</b>	<b>78.7</b>	79.8	63.6	<b>56.6</b>	<b>63.6</b>

## D. Additional Domain Adaptations

**Cityscapes  $\rightarrow$  Foggy Cityscapes** Table 18 shows the result for domain adaptative object detection from Cityscapes  $\rightarrow$  Foggy Cityscapes.

## E. Additional Analysis

**Pixel Accuracy Visualizations** Figure 11 show per-pixel accuracy visualization. For both Cityscapes [4] and ACDC [32], a noticeable predominance of red over blue is observed, showing a clear advantage of our method upon DAFormer [12] for semantic segmentation.

**BDD100K Clear  $\rightarrow$  Rainy Object Detection.** Qualitative comparisons are shown in Figure 12. Our method demonstrates superior object detection under rainy conditions by accurately identifying vehicles and minimizing false positives, such as the misidentified pedestrians and cars evident in the 2PCNet [17] predictions.

**Cityscapes  $\rightarrow$  DarkZurich Semantic Segmentation.** Qualitative comparisons are shown in Figure 13. The proposed method exhibits a segmentation output that is more closely aligned with groundtruth, particularly while predict-

ing road boundaries and consistently identification of urban elements such as sidewalk, terrain, and traffic signs. This indicates that our method has superior domain adaptation capabilities in challenging low-light conditions.

## F. Additional Technical Details

**Ground Truth Segmentation to Boxes:** Instance-based image warping requires bounding boxes, which are not provided in some semantic segmentation benchmarks like GTA [28]. To circumvent this, we generate “from-seg” bounding boxes from ground truth semantic segmentation maps. We do this by identifying connected components that represent individual instances of foreground categories — specifically, traffic lights, traffic signs, persons, riders, cars, trucks, buses, trains, motorcycles, and bikes.

For each “from-seg” instance, we compute the bounding boxes by finding the minimum enclosing axis-aligned rectangle. These “from-seg” bounding boxes are then employed for instance-level image warping in a similar manner to ground truth bounding boxes.

Table 10. **Synthetic to Real Domain Adaptation: Synthia → Cityscapes Semantic Segmentation.** Tested on Cityscapes Val. We were unable to reproduce DAFormer’s [12] results averaged over 3 random seeds, hence we present results with seed=0 for both DAFormer [12] and our method (DAFormer with Instance-level Image Warping). *We do not target adaptation from synthetic datasets and Sim2Real Domain Gap, as synthetic datasets may not have a scale bias.* Our improvement on Synthia → Cityscapes are marginal and we believe this is because *Synthia does not exhibit scale bias akin to natural driving scenes* (See Figure 9).

Method	mIoU	road	side walk	building	wall	fence	pole	traffic light	traffic sign	vegetation	terrain	sky	person	rider	car	truck	bus	train	motor cycle	bike
CBST [50]	42.6	68.0	29.9	76.3	10.8	1.4	33.9	22.8	29.5	77.6	-	78.3	60.6	28.3	81.6	-	23.5	-	18.8	39.8
DACS [38]	48.3	80.6	25.1	81.9	21.5	2.9	37.2	22.7	24.0	83.7	-	<b>90.8</b>	67.6	38.3	82.9	-	38.9	-	28.5	47.6
CorDA [41]	55.0	<b>93.3</b>	<b>61.6</b>	85.3	19.6	5.1	37.8	36.6	42.8	<b>84.9</b>	-	90.4	69.7	41.8	85.6	-	38.4	-	32.6	53.9
ProDA [48]	55.5	87.8	45.7	84.6	37.1	0.6	44.0	54.6	37.0	<b>88.1</b>	-	84.4	<b>74.2</b>	24.3	88.2	-	51.1	-	40.5	45.6
DAFormer [12]	<b>60.9</b>	84.5	40.7	<b>88.4</b>	41.5	6.5	<b>50.0</b>	<b>55.0</b>	<b>54.6</b>	86.0	-	89.8	73.2	<b>48.2</b>	87.2	-	<b>53.2</b>	-	53.9	61.7
DAFormer (seed=0)	59.2	87.8	47.6	87.6	43.7	5.8	49.0	48.0	53.1	82.3	-	71.8	71.7	46.0	87.5	-	49.3	-	52.7	<b>63.4</b>
+ Ours	59.4	92.7	57.7	87.1	<b>44.8</b>	<b>7.1</b>	46.2	46.9	53.6	80.6	-	68.2	72.5	42.5	<b>90.6</b>	-	41.6	-	<b>55.2</b>	63.3

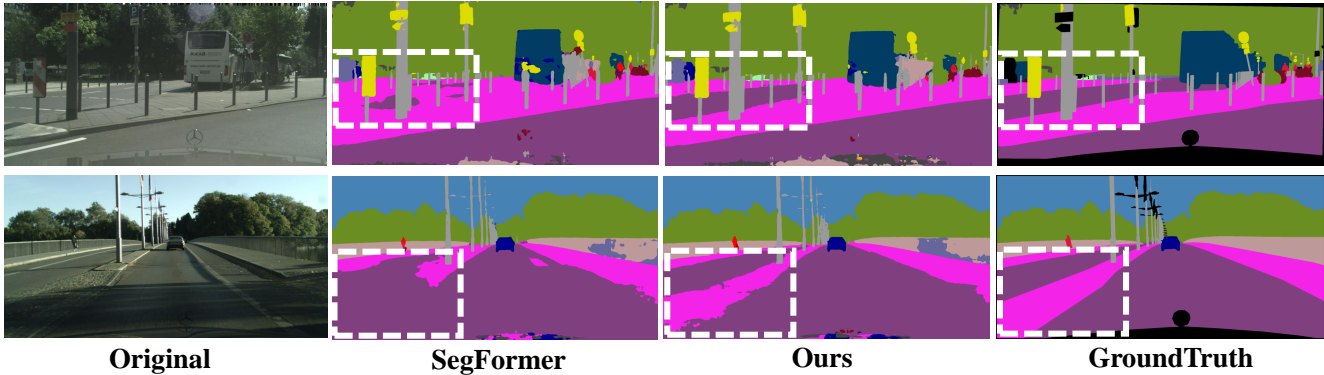


Figure 10. **Supervised Setting: Visual Comparison on Cityscapes Semantic Segmentation.** Our segmentation map more closely resembles the ground truth, indicating a more accurate understanding of the urban scene. Notably, our method effectively distinguishes categories such as sidewalks and roads, despite the presence of occlusions (top row) and shadows (bottom row).

Table 11. **Comparison with other Domain Adaptation Strategies: Computational Overheads.** We are using a single RTX 4090 GPU. The batch size is 1, and all the other training and inference configuration are the same their respective papers – DAFormer [12] and HRDA [13]. Instance-level image warping imposes minimal memory overheads during training. Moreover, as we do not warp during test time, our method does not have any inference latency overheads.

Method	Training Memory	Inference Time
DAFormer	16.41 GB	195.0 ms
DAFormer + Ours	+ 0.04 GB	+ 0 ms
DAFormer + HRDA	+ 5.11 GB	+ 801.2 ms

Table 12. **Comparison with other Domain Adaptation Strategies: Cityscapes → DarkZurich Semantic Segmentation.** Tested on DarkZurich Val. Our method improves IoU scores in conjunction with both DAFormer and MIC (HRDA) strategies. We observe smaller improvements with MIC (HRDA) as HRDA uses multi-scale cropping strategy, which alleviates scale bias to some extent.

Method	mIoU	road	side walk	building	wall	fence	pole	traffic light	traffic sign	vegetation	terrain	sky	person	rider	car	truck	bus	train	motor cycle	bike
DAFormer	33.8	<b>92.0</b>	66.7	47.3	25.9	<b>50.8</b>	38.0	24.6	19.4	<b>62.2</b>	31.9	17.9	20.4	<b>28.4</b>	61.7	-	-	-	21.0	<b>34.3</b>
DAFormer + Ours	<b>37.1</b>	88.7	<b>70.9</b>	<b>60.1</b>	<b>42.1</b>	49.6	<b>39.8</b>	<b>47.9</b>	<b>21.5</b>	49.8	<b>35.7</b>	<b>25.4</b>	<b>23.8</b>	25.9	<b>66.8</b>	-	-	-	<b>24.3</b>	32.4
MIC (HRDA)	39.8	<b>78.8</b>	<b>13.0</b>	83.1	46.7	52.2	42.2	<b>44.5</b>	28.8	64.3	35.4	<b>82.8</b>	24.9	<b>33.8</b>	62.8	-	-	-	<b>25.9</b>	<b>37.3</b>
MIC (HRDA) + Ours	<b>40.1</b>	75.8	5.8	<b>83.3</b>	<b>55.7</b>	<b>54.8</b>	<b>44.3</b>	30.5	<b>38.0</b>	<b>66.3</b>	<b>42.7</b>	82.4	<b>39.4</b>	15.1	<b>69.3</b>	-	-	-	25.1	32.9

Table 13. **Comparison with other Domain Adaptation Strategies: Cityscapes → ACDC Semantic Segmentation.** Tested on ACDC Val. Our method achieves a significant improvement in the IoU score in conjunction with both DAFormer and MIC (HRDA) strategies. We observe smaller improvements with MIC (HRDA) as HRDA uses multi-scale cropping strategy, which alleviates scale bias to some extent.

Method	mIoU	road	side walk	building	wall	fence	pole	traffic light	traffic sign	vegetation	terrain	sky	person	rider	car	truck	bus	train	motor cycle	bike
DAFormer	57.6	72.7	<b>57.5</b>	<b>80.1</b>	42.5	38.0	50.9	45.1	50.0	71.1	<b>38.5</b>	67.0	56.0	29.9	81.8	76.6	78.9	79.9	40.8	36.7
DAFormer + Ours	<b>61.8</b>	<b>82.9</b>	56.1	79.8	<b>44.6</b>	<b>40.3</b>	<b>52.7</b>	<b>60.8</b>	<b>52.5</b>	<b>72.0</b>	38.4	<b>78.0</b>	<b>56.6</b>	<b>30.5</b>	<b>84.9</b>	<b>80.2</b>	<b>86.9</b>	<b>86.4</b>	<b>44.5</b>	<b>45.8</b>
MIC (HRDA)	59.6	66.4	<b>55.8</b>	<b>84.8</b>	<b>54.6</b>	<b>41.3</b>	49.7	41.2	<b>53.6</b>	<b>78.3</b>	37.7	67.4	58.3	24.0	83.6	70.1	88.8	87.9	<b>40.7</b>	48.4
MIC (HRDA) + Ours	<b>61.6</b>	<b>80.6</b>	38.6	83.7	50.5	<b>41.3</b>	<b>50.5</b>	<b>56.7</b>	49.6	75.2	<b>39.4</b>	<b>83.9</b>	<b>58.9</b>	<b>32.0</b>	<b>86.0</b>	<b>75.4</b>	<b>91.8</b>	<b>88.0</b>	40.2	<b>48.5</b>

Table 14. **Comparison with other Domain Adaptation Strategies: Ablation on Cityscapes → ACDC Semantic Segmentation.** Tested on ACDC Val. We show that our method improves performance in conjunction with base DAFormer [12], MIC [14], HRDA [13] and HRDA without HR-detail crop (HRDA\*) respectively. Our observations are – (a) Instance-level image warping improves MIC, however, fails to improve beyond DAFormer with instance-level image warping. – (b) HRDA performs worse than DAFormer at DAFormer’s training scales, showing that full resolution training is needed for HRDA to perform well, consistent with [13]. Our method only improves marginally as both methods try to alleviate scale biases. – (c) As we train with DAFormer’s training scales to maintain fairness, removing the HR-detail crop is beneficial as the expected cropped size is small. Adding instance-level image warping to focus on small object details instead of a detail crop, in conjunction with HRDA’s context crop improves performance considerably.

Method	mIoU	road	side walk	building	wall	fence	pole	traffic light	traffic sign	vegetation	terrain	sky	person	rider	car	truck	bus	train	motor cycle	bike
DAFormer	57.6	72.7	<b>57.5</b>	<b>80.1</b>	42.5	38.0	50.9	45.1	50.0	71.1	<b>38.5</b>	67.0	56.0	29.9	81.8	76.6	78.9	79.9	40.8	36.7
DAFormer + Ours	<b>61.8</b>	<b>82.9</b>	56.1	79.8	<b>44.6</b>	<b>40.3</b>	<b>52.7</b>	<b>60.8</b>	<b>52.5</b>	<b>72.0</b>	38.4	<b>78.0</b>	<b>56.6</b>	<b>30.5</b>	<b>84.9</b>	<b>80.2</b>	<b>86.9</b>	<b>86.4</b>	<b>44.5</b>	<b>45.8</b>
MIC (DAFormer)	58.8	61.1	59.5	73.2	<b>47.4</b>	<b>45.2</b>	51.4	44.7	48.2	<b>78.4</b>	38.1	51.4	60.4	<b>41.3</b>	84.3	78.5	84.3	78.9	<b>43.9</b>	<b>46.5</b>
MIC (DAFormer) + Ours	<b>60.6</b>	<b>72.8</b>	<b>62.9</b>	<b>73.4</b>	45.1	36.5	<b>52.9</b>	<b>49.0</b>	<b>49.9</b>	76.9	<b>39.8</b>	<b>65.5</b>	<b>60.6</b>	40.4	<b>85.2</b>	<b>80.9</b>	<b>90.5</b>	<b>87.0</b>	41.0	41.3
HRDA (DAFormer)	56.9	79.9	37.8	<b>81.1</b>	<b>45.6</b>	33.9	47.8	<b>47.3</b>	47.1	74.3	37.1	<b>84.0</b>	47.7	17.6	<b>84.2</b>	69.1	88.2	75.1	37.6	45.1
HRDA (DAFormer) + Ours	<b>57.7</b>	<b>85.6</b>	<b>48.2</b>	71.7	41.6	<b>39.4</b>	<b>50.8</b>	17.7	<b>47.8</b>	<b>75.2</b>	<b>37.9</b>	81.4	<b>56.3</b>	<b>25.0</b>	<b>82.3</b>	<b>73.4</b>	<b>88.8</b>	<b>82.3</b>	<b>45.3</b>	<b>46.7</b>
HRDA* (DAFormer)	58.3	68.5	59.4	82.8	<b>50.4</b>	<b>40.8</b>	50.3	42.4	44.4	<b>77.6</b>	38.0	69.4	<b>55.7</b>	27.2	83.2	77.4	78.2	79.0	34.9	48.4
HRDA* (DAFormer) + Ours	<b>62.1</b>	<b>89.7</b>	<b>61.1</b>	<b>83.9</b>	43.4	39.5	<b>52.7</b>	<b>43.1</b>	<b>45.0</b>	75.6	<b>38.7</b>	<b>86.1</b>	55.0	<b>28.0</b>	<b>84.9</b>	<b>81.1</b>	<b>88.5</b>	<b>86.0</b>	<b>44.9</b>	<b>53.4</b>

Table 15. **Supervised Setting: Cityscapes Semantic Segmentation.** Tested on Cityscapes Val. Our instance-level image warping also improves segmentation on source domain by **+1.5 mIoU** (along with target domain, See results on Table 4 and 5 in the main manuscript), implying that learned backbone features are better.

Method	mIoU	road	side walk	building	wall	fence	pole	traffic light	traffic sign	vegetation	terrain	sky	person	rider	car	truck	bus	train	motor cycle	bike
SegFormer	75.3	98.0	83.4	91.8	59.6	59.6	57.5	64.0	74.4	91.9	62.8	94.6	77.6	56.0	93.7	81.6	81.4	70.1	59.2	73.3
+ Ours w/ Sta. Prior	76.1	97.9	83.6	91.9	58.0	58.0	57.7	63.3	73.9	91.7	64.4	94.4	77.7	<b>57.4</b>	93.8	81.0	<b>87.7</b>	80.3	60.7	72.8
+ Ours w/ Geo. Prior	76.5	98.0	84.3	<b>92.2</b>	<b>61.4</b>	57.6	59.3	64.7	74.0	91.9	65.3	94.7	78.2	55.3	93.9	<b>83.1</b>	86.5	81.1	60.1	72.1
+ Ours w/ Inst.	<b>76.8</b>	<b>98.1</b>	<b>84.8</b>	<b>92.2</b>	59.9	<b>58.3</b>	<b>59.6</b>	<b>65.1</b>	<b>75.4</b>	<b>92.3</b>	<b>66.2</b>	<b>94.8</b>	<b>78.2</b>	55.3	<b>94.2</b>	82.0	85.7	<b>81.3</b>	<b>61.8</b>	<b>74.4</b>

Table 16. **Supervised Setting: BDD100K (Day) Object Detection.** Tested on BDD100K Day Val. Day images here include both images captured in good and bad weather. As shown by mAP50 (overall and per category), our method improves detection performance in the source domain while our saliency guidance is competitive with other saliency priors.

Method	mAP	mAP50	mAP75	mAPs	mAPm	mAPI	person	rider	car	truck	bus	motor cycle	bike	traffic light	traffic sign
FRCNN	30.1	56.4	28.1	13.9	37.6	51.0	64.0	50.7	80.3	62.5	62.9	45.3	49.7	66.7	69.8
+ Ours w/ Sta. Prior	30.9	57.1	<b>28.6</b>	14.4	<b>38.9</b>	<b>53.4</b>	65.7	53.1	<b>80.9</b>	<b>62.7</b>	63.0	<b>48.8</b>	50.8	<b>69.2</b>	71.2
+ Ours w/ Geo. Prior	<b>31.1</b>	<b>57.9</b>	28.3	<b>14.5</b>	38.5	52.7	66.3	<b>53.6</b>	80.7	62.5	62.8	48.1	<b>52.9</b>	68.4	<b>71.4</b>
+ Ours w/ Inst.	30.7	57.2	27.9	<b>14.5</b>	38.4	52.8	<b>66.4</b>	53.3	80.8	62.4	<b>63.7</b>	47.7	51.7	68.6	71.1



Table 17. **Supervised Setting: BDD100K (Clear) Object Detection.** Tested on BDD100K Clear Val. Clear images here include both day and night images. As shown by mAP50 (overall and per category), our method improves detection performance in the source domain while our saliency guidance is competitive with other saliency priors.

Method	mAP	<b>mAP50</b>	mAP75	mAPs	mAPm	mAPI	person	rider	car	truck	bus	motor cycle	bike	traffic light	traffic sign
FRCNN	25.4	49.6	22.5	12.2	30.3	44.2	59.3	38.8	76.5	53.2	54.7	43.1	45.6	56.4	68.7
+ Ours w/ Sta. Prior	<b>26.0</b>	50.2	<b>22.9</b>	11.9	<b>31.2</b>	44.5	59.2	38.8	<b>76.7</b>	<b>54.5</b>	55.7	<b>45.5</b>	46.0	56.6	69.2
+ Ours w/ Geo. Prior	25.9	<b>50.3</b>	22.8	12.0	31.0	<b>44.8</b>	59.4	<b>41.1</b>	<b>76.7</b>	53.7	56.1	42.7	<b>46.9</b>	<b>56.7</b>	<b>69.3</b>
+ Ours w/ Inst.	25.9	50.1	22.8	<b>12.2</b>	31.0	43.7	<b>59.7</b>	37.7	76.6	54.4	<b>56.9</b>	43.7	46.0	56.5	69.1

Table 18. **Additional Domain Adaptations: Cityscapes → Foggy Cityscapes.** Cityscapes and Foggy Cityscapes both feature identical backgrounds, resulting in a shared scale bias. However, the *synthetic* fog introduced in Foggy Cityscapes does not accurately mimic the properties of real fog, thereby posing less of a challenge to segmentation algorithms. As a result, the baseline model already attains high scores on the Foggy Cityscapes dataset, making it difficult for our warping method to yield substantial additional improvements.

Method	<b>mIoU</b>	road	side walk	building	wall	fence	pole	traffic light	traffic sign	vegetation	terrain	sky	person	rider	car	truck	bus	train	motor cycle	bike
DAFormer	74.7	97.8	83.0	88.7	<b>60.4</b>	59.4	57.4	<b>60.7</b>	72.8	89.2	<b>64.9</b>	81.2	76.6	54.4	<b>93.2</b>	75.9	86.9	80.7	62.8	73.8
+ Ours w/ Inst.	<b>75.5</b>	<b>98.0</b>	<b>84.2</b>	<b>89.7</b>	59.7	<b>61.9</b>	<b>57.7</b>	60.4	<b>73.3</b>	<b>89.4</b>	62.2	<b>82.4</b>	<b>76.7</b>	<b>56.3</b>	92.8	<b>82.2</b>	<b>88.0</b>	<b>82.0</b>	<b>63.5</b>	<b>73.9</b>

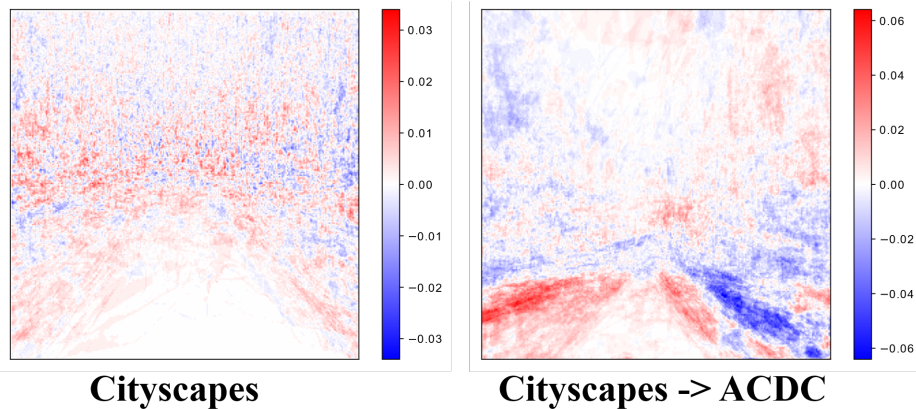


Figure 11. **Visualization of the per-pixel accuracy difference between the baseline and our method.** Red indicates our method is better, whereas blue means the baseline is better. The comparison for the ‘sky’ class has been omitted, and the semantic segmentation maps are reshaped to  $256 \times 256$  to improve the quality of the visualization. We can see that our method outperforms the baseline across most pixels, with the exception of right-hand side sidewalk pixels in the ACDC dataset (blue band) due to a significant disparity in sidewalk width compared to the Cityscapes dataset.



Figure 12. **Additional Analysis: BDD100K (clear → rainy) Object detection.** Our method demonstrates superior object detection under rainy conditions by accurately identifying vehicles and minimizing false positives, such as the misidentified pedestrians (persons) and cars evident in 2PCNet [17] predictions.

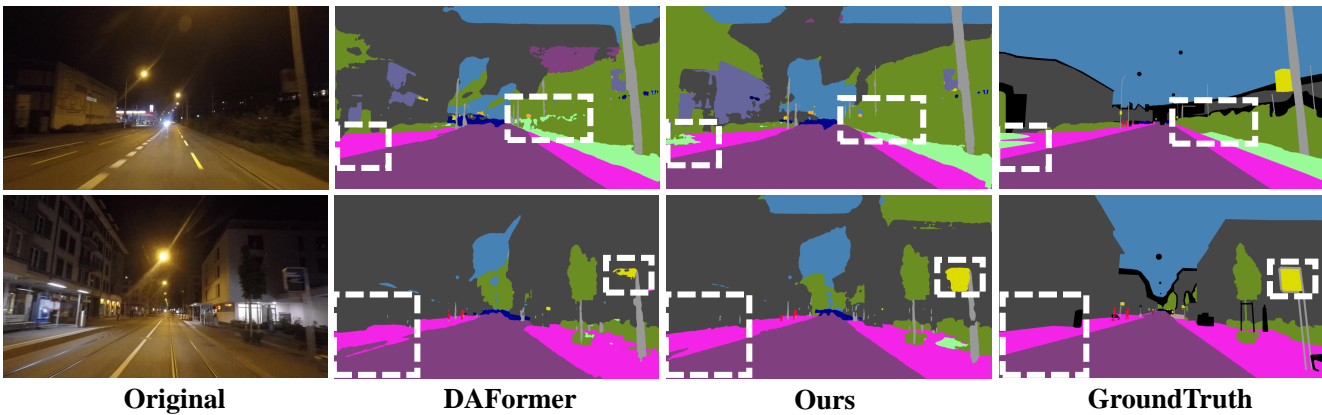


Figure 13. **Additional Analysis: Cityscapes → DarkZurich Semantic Segmentation.** The proposed method exhibits a segmentation output that is more closely aligned with the groundtruth, particularly in the accurate predictions of road boundaries and consistent identification of urban elements such as sidewalk, terrain, and traffic signs. This indicates that our method has superior domain adaptation capabilities in the challenging low-light conditions.